(Invitrogen) containing full-length Munc13-4 using LipofectAMINE (Invitrogen).

Assay Analyzing Direct Interaction of Munc13-4 with Rab27—Binding of Munc13-4 with small GTPases was carried out by affinity chromatography. Glutathione-Sepharose beads coated with GTPγS- or GDP-bound Rab GTPases (each 1 μg) were prepared by incubation for 1 h at 4 °C in Buffer A. Then the prepared beads were incubated with purified 0.5 μg of His_6-Munc13-4 for 1 h at 4 °C in Buffer A and washed three times with Buffer A at 4 °C. Bead-associated His_6-Munc13-4 was analyzed by immunoblotting with anti-Munc13-4 antibody.

Density Gradient Separation of Platelet Organelles—We first loaded [^{3}H]serotonin into dense core granules of platelets from 50 ml of freshly obtained blood and permeabilized the platelets with SLO. Then, after centrifugation to remove most of cytosol and resuspension in 1 ml of Buffer A containing the ATP regeneration system, the platelets were disrupted by sonication and centrifuged at 600 × *g* for 5 min to remove unbroken platelets. The supernatant was layered on the top of metrizamide stepwise gradient (each 1.0-ml layer at 1.30–1.00 g/ml in density decreasing by each 0.03 g/ml from the bottom) in Buffer A containing the ATP regeneration system and centrifuged at 28,000 rpm with Beckman Rotor SW40 for 2 h at 4 °C as described (31). Aliquots of the fractions were analyzed by Western blot with indicated antibodies and counting radioactivity of [^{3}H]serotonin. The separation of the membrane and cytosolic fraction was performed by centrifugation at 300,000 × *g* for 30 min at 4 °C after disrupting platelets by sonication or at 600 × *g* for 5 min after the SLO permeabilization of platelets.

RESULTS

Unprenylated Rab27 Inhibits the Ca^{2+}-induced Dense Core Granule Secretion—In the present study, we used a previously established *in vitro* assay system using SLO-permeabilized platelets by monitoring secreted [^{3}H]serotonin preloaded into dense core granules (31, 32, 35). Agonists promote granule secretions by increasing intracellular calcium ion concentrations in platelets (36). Upon permeabilization of platelets the intracellular and extracellular concentrations of calcium are equal; therefore we used calcium chloride as a stimulus. In the assay, the secretion of the granules was reconstituted by the addition of ATP and exogenous platelet cytosol, and the response observed was equivalent to intact platelets in the time course and the Ca^{2+} sensitivity (31, 32, 35).

Small GTPases produced in *E. coli* are not modified by the addition of prenyl groups at their C termini (37), which is essential for the correct localization and activity (2, 3, 38). Incubation of permeabilized platelets with Rab27A and Rab27B purified from *E. coli* inhibited the Ca^{2+}-induced dense core granule secretion in a concentration-dependent manner (Fig. 1*A*). Incubation of permeabilized platelets with other small GTPases such as Rab3B, Rab4B, Rab5A, or Rap1B, a Ras family small GTPase whose GTP-bound form has been shown to be increased upon platelet activation (39), had no effect (Fig. 1*B*), indicating that the effect of Rab27 is specific. We prepared and purified mutant Rab27A-T23N, which preferentially binds GDP, and Rab27A-Q78L, which lacks GTPase activity (40). Incubation of permeabilized platelets with Rab27A-Q78L, but not Rab27A-T23N, inhibited the secretion in a concentration-dependent manner (Fig. 1*C*). Inhibition by unprenylated Rab27A-Q78L, wild type Rab27A, and Rab27B could be due to sequestration of putative Rab27 effector molecules from endogenous membrane-associated GTP-Rab27 by forming nonfunctional complexes with effector proteins. These data demonstrate that Rab27 is involved in the regulation of dense core granule secretion in platelets.

Identification of Munc13-4 as a GTP-Rab27-binding Protein in Platelet Cytosol—To elucidate the mechanism of action of Rab27, we attempted to identify GTP-Rab27-binding proteins that might mediate the function of Rab27 in the granule secretion, from platelet cytosol by affinity chromatography. As shown in Fig. 2*A*, we detected one major protein migrating at ~120 kDa on GTPγS-GST-Rab27A beads (*lane 4*) but not on GDP-GST-Rab27A- (lane 5) or GST beads (*lane 3*). TOF-MS analysis of the protein and a data base search revealed that the 120-kDa protein was the human homologue of rat Munc13-4 (24) because most of the peptide masses obtained by the TOF-MS analysis were detected all over the human Munc13-4 molecule (Fig. 2*B*). Human Munc13-4 consists of 1,090 amino acids, and the primary structure is 88% identical to that of rat Munc13-4. As is the case with Munc13-1–3, Munc13-4 contains two calcium-binding C2 domains and Munc13 homology do-

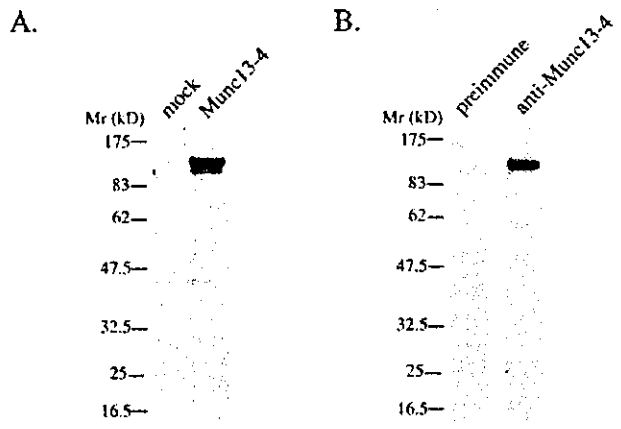

FIG. 3. **Anti-Munc13-4 antibody recognizes a single band at 120 kDa in platelet lysate.** *A*, Munc13-4- and mock-transfected HeLa cell lysates were immunoblotted with the anti-Munc13-4 antibody as described under "Experimental Procedures." *B*, platelet lysates were immunoblotted with preimmune serum and the anti-Munc13-4 antibody as described under "Experimental Procedures." The data shown are the representative of three independent experiments with similar results.

FIG. 4. **Direct interaction of recombinant Munc13-4 with GTPγS-Rab27 *in vitro*.** *A*, recombinant His_6-Munc13-4 was produced and purified from the over-expressing Sf9 cells and analyzed by SDS-PAGE gel stained by Coomassie Blue as described under "Experimental Procedures." *B*, glutathione beads coated with GTPγS- or GDP-bound various GST-Rab GTPases (each 1 μg) were incubated with His_6-Munc13-4 (0.5 μg) *in vitro*, and the bead-associated His_6-Munc13-4 was detected by Western blotting with anti-His_6 antibody as described under "Experimental Procedures." Purified Munc13-4 used for the affinity analysis is also shown (10% of load). The data shown are representative of three independent experiments with similar results.

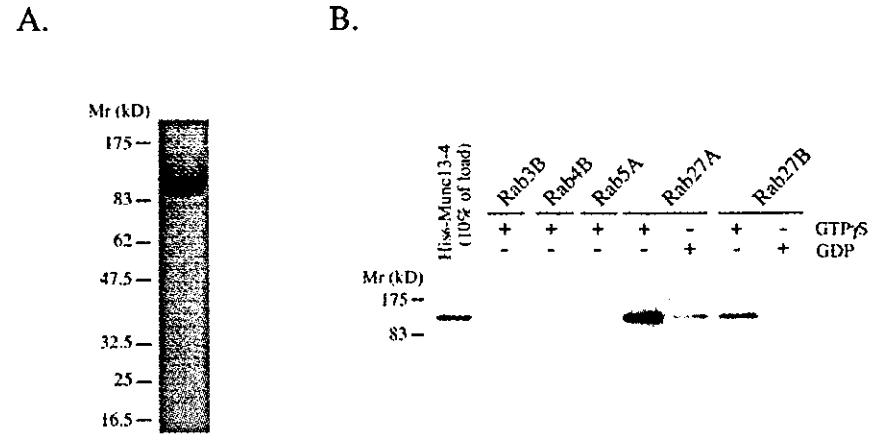

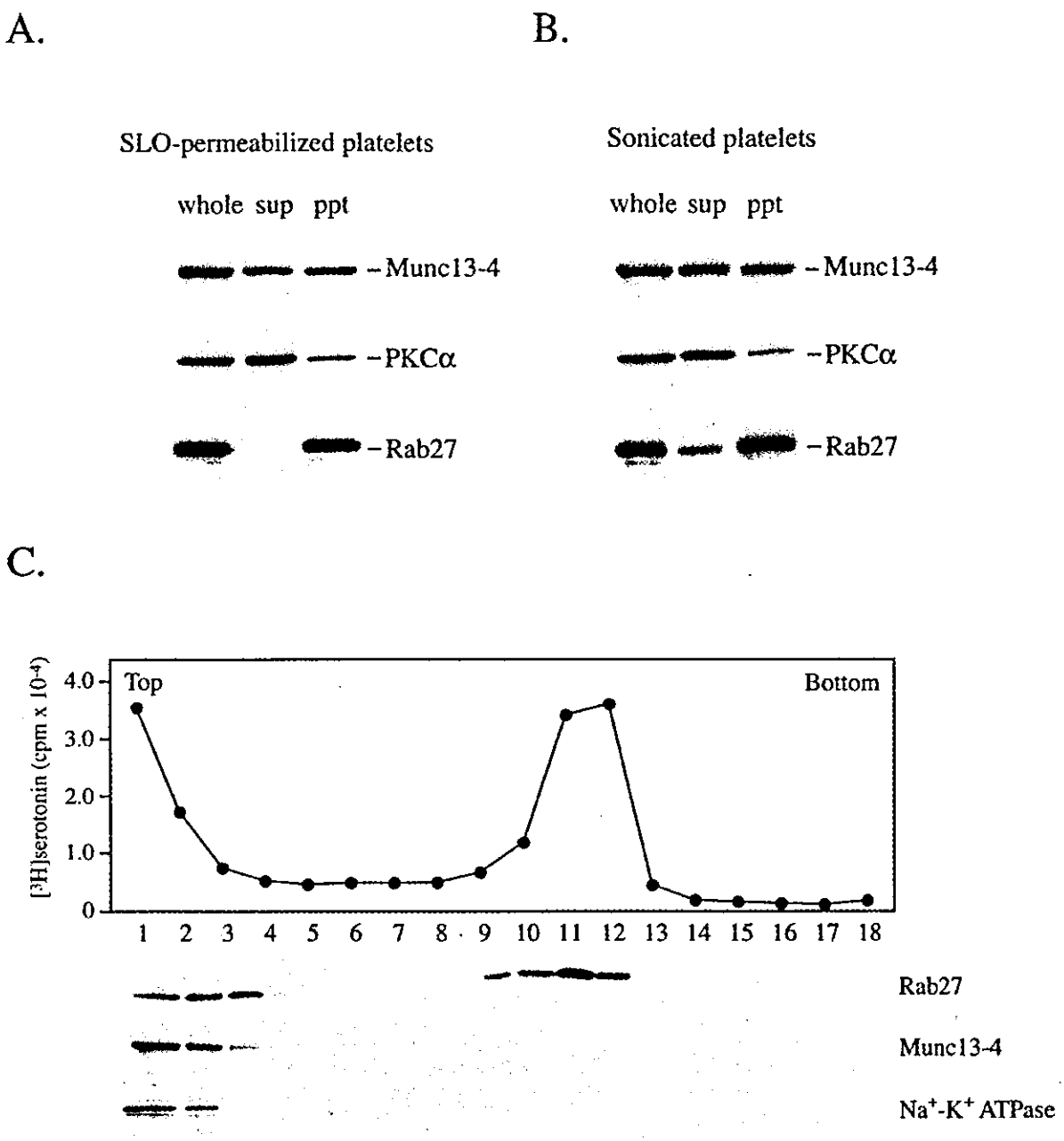

FIG. 5. **Localization of Munc13-4 in platelet organelles.** *A* and *B*, after centrifugation of isolated platelets permeabilized with SLO for 30 min (*A*) or sonicated directly (*B*), comparable amounts of the supernatant (*sup*) and pellets (*ppt*) were analyzed by immunoblotting with anti-Munc13-4, anti-PKCα, and anti-Rab27 antibodies as described under "Experimental Procedures." The data shown are the representative of three independent experiments with similar results. *C*, after separation of organelles of [^{3}H]serotonin-loaded permeabilized platelets by density gradient, [^{3}H]serotonin was measured by a liquid scintillation counter and Munc13-4, Rab27, and Na,K-ATPase were detected by immunoblotting in each fraction as described under "Experimental Procedures." The data shown are the representative of three independent experiments with similar results.

mains, whereas Munc13-4 lacks the long N-terminal region containing a phorbol ester-binding C1 domain present in Munc13-1–3 (21, 24) (Fig. 2*C*).

We generated an antibody against the N-terminal region of human Munc13-4 (residues 1–262). The antibody recognized a 120-kDa protein in HeLa cells transfected with Munc13-4 but not in mock transfected cells (Fig. 3*A*). The antibody recognized a single band at 120 kDa in platelet lysate (Fig. 3*B*) and also the 120-kDa protein eluted from the GTPγS-GST-Rab27A-loaded affinity chromatography column (data not shown), confirming that the 120-kDa protein that we identified is indeed Munc13-4.

To examine whether the interaction of Munc13-4 with Rab27 is direct, we produced and purified full-length His_6-Munc13-4 using the baculovirus expression system in Sf9 insect cells (Fig. 4*A*). As shown in Fig. 4*B*, recombinant Munc13-4 could bind directly to GTPγS-Rab27A but only slightly to GDP-Rab27A *in vitro*. Furthermore, Munc13-4 demonstrated a weaker interaction with GTPγS-Rab27B, compared with GTPγS-Rab27A. Importantly, Munc13-4 did not bind to GTPγS-Rab3B, -Rab4B, or -Rab5A (Fig. 4*B*). Thus, the interaction of Munc13-4 with Rab27 is direct, GTP-dependent, and specific.

Localization of Munc13-4—Munc13-1 has been demon-

strated to localize specifically to the presynaptic plasma membrane, although it does not contain a membrane-spanning region (20). Munc13-4 also lacks a transmembrane region. We examined the subcellular localization of Munc13-4 in platelets. As shown in Fig. 5*A*, Munc13-4 was equally distributed between the cytosolic and membrane fractions in SLO-permeabilized platelets, whereas Rab27 was exclusively membrane-associated. As expected, PKCα was found predominantly in the soluble supernatant fraction (Fig. 5*A*). When isolated platelets were directly sonicated and centrifuged at 300,000 × *g*, localization of Munc13-4, Rab27, and PKCα was similar to the results in the SLO-permeabilized platelets (Fig. 5*B*). Namely, ~50% of Munc13-4, most of Rab27, and a small part of PKCα were recovered in the pellet after the high speed centrifugation (Fig. 5*B*), suggesting a strong affinity of Munc13-4 to the membrane.

Next, we biochemically examined the localization of Rab27 and membrane-associated Munc13-4 in platelet organelles. We first loaded [^{3}H]serotonin into dense core granules of platelets and permeabilized the platelets with SLO. Then, after centrifugation to remove cytosol, the cytosol-depleted platelets were disrupted by sonication, and the low speed supernatant containing platelet organelles was separated by a density gradient method (31). As shown in Fig. 5*C*, [^{3}H]serotonin was recovered in two peaks. The lighter peak is presumably due to [^{3}H]serotonin leaking from the dense core granules. The heavier fractions of [^{3}H]serotonin indicate the presence of dense core granules. The majority of Rab27 was recovered together with fractions of dense core granules containing [^{3}H]serotonin, whereas some Rab27 was detected in the low density fractions where a plasma membrane marker Na,K-ATPase was recovered (Fig. 5*C*). Under these conditions, Munc13-4 was recovered in the lighter fractions together with Na,K-ATPase but not in the vesicle fractions (Fig. 5*C*), suggesting that Munc13-4 is on the plasma membrane but not on the dense core granules in platelets.

Involvement of Munc13-4 in the Regulation of Dense Core Granule Secretion—We finally examined whether Munc13-4 regulates dense core granule secretion in platelets using the semi-intact secretion assay. In basal conditions, SLO-permeabilized platelets retained a residual amount of membrane-associated Munc13-4 (Fig. 5*A*), and exogenously added platelet cytosol contained 80 nM Munc13-4. Under these conditions, the addition of purified Munc13-4 (Fig. 4*A*) enhanced the Ca^{2+}-induced secretion of dense core granules in a concentration-dependent manner (Fig. 6*A*). The activity of Munc13-4 was abolished when Munc13-4 was denatured (Fig. 6*A*), suggesting that the activity was not due to a nonspecific effect of the buffer. The dense core granule secretion was time-dependent, and the addition of Munc13-4 not only accelerated the kinetics but also increased the amounts of the secretion (Fig. 6*B*). Importantly, the inhibition of secretion by unprenylated Rab27A was rescued by the addition of recombinant Munc13-4 in a concentration-dependent manner (Fig. 6*C*).

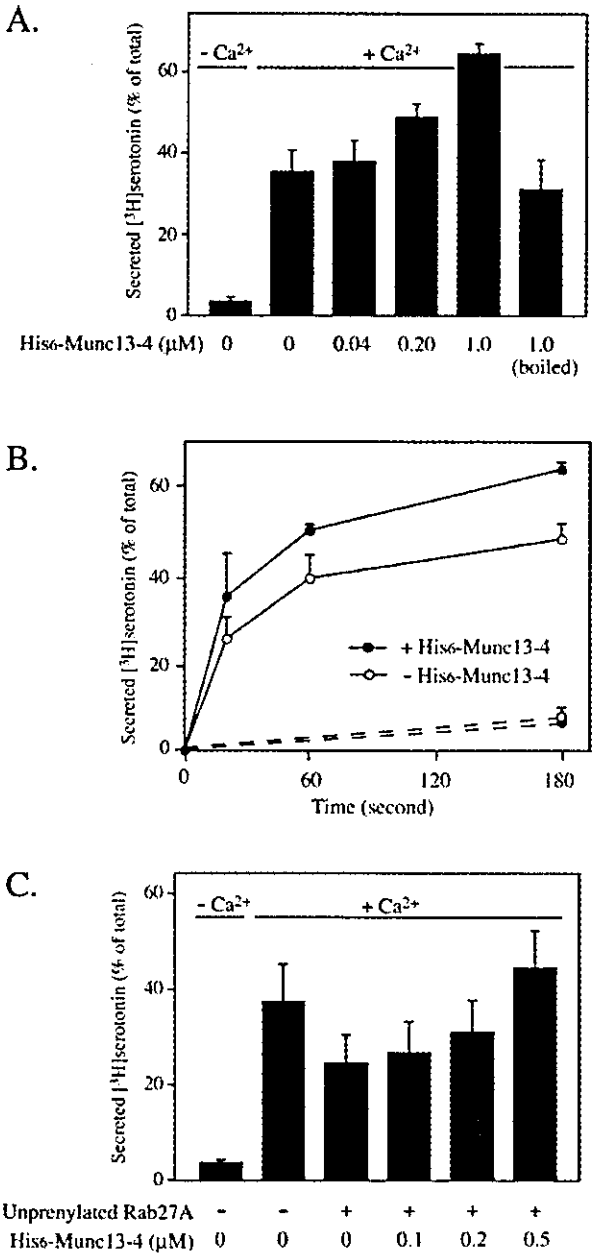

FIG. 6. **Munc13-4 enhances the dense core granule secretion and rescues the inhibition by unprenylated Rab27A.** *A*, permeabilized platelets were first incubated with the indicated concentrations of Munc13-4, and the Ca^{2+}-induced secretion of dense core granules for 1 min was analyzed in the standard assay condition by measuring secreted [^{3}H]serotonin preloaded in dense core granules as described under "Experimental Procedures." *B*, permeabilized platelets were first incubated in the absence (*open circles*) or the presence (*closed circles*) of 0.2 μM Munc13-4 and then incubated with Ca^{2+} at 20 nM (*broken lines*) or 20 μM (*solid lines*) for the indicated periods. The Ca^{2+}-induced secretion of dense core granules for indicated periods was analyzed as described under "Experimental Procedures." *C*, permeabilized platelets were first incubated in the absence or presence of unprenylated Rab27A at 2.0 μM with various concentrations of Munc13-4. The Ca^{2+}-induced secretion of dense core granules for 1 min was analyzed as described under "Experimental Procedures." The results shown are expressed as the means ± S.E. of three independent experiments.

DISCUSSION

Here we have demonstrated that Rab27 regulates the Ca^{2+}-induced dense core granule secretion in platelets by showing that the addition of unprenylated dominant active Rab27A, wild type Rab27A, and Rab27B but not other GTPases inhibited the secretion in permeabilized platelets. In addition, we identified Munc13-4 as a novel GTP-Rab27-binding protein. We further demonstrated that Munc13-4 mediates the function of GTP-Rab27 in the regulation of the secretion by showing that the addition of Munc13-4 enhanced the secretion and rescued the inhibition of secretion by unprenylated Rab27.

We have shown that the addition of unprenylated Rab27 purified from *E. coli* inhibited the Ca^{2+}-induced dense core granule secretion. In the secretion assay, added unprenylated Rab27 is theoretically unable to localize to the membrane and therefore would sequester Rab27 effector molecules by forming

nonfunctional complexes. Unprenylated Rab27A-T23N with preferential GDP binding would act as a dominant negative protein when expressed in cells (41). However, here we observed almost no effect of Rab27A-T23N on the dense core granule secretion in our semi-intact system (Fig. 1*C*). On the other hand, unprenylated GTPase-deficient mutant Rab27A-Q78L inhibited the secretion to a similar extent as wild type Rab27A and Rab27B. This could depend upon the ability of association with effector molecules of Rab27. The mechanism might be similar to that seen in the inhibition of the insulin signaling in adipocytes by overexpression of prenylation-deficient Rab4 (42). Thus, GTP-Rab27 is essential for dense core granule secretion in platelets once the granules are normally generated, although there is controversy concerning the role of Rab27 in dense core granule biogenesis (4, 13, 14).

To identify specific GTP-Rab27-binding protein(s) that may function in dense core granule secretion in platelets, we performed Rab27 affinity chromatography using platelet cytosol as the source for interacting proteins. We detected a GTPγS-Rab27A-binding protein at 120 kDa and identified it as the human homologue of rat Munc13-4 (24) by TOF-MS analysis and a data base search. Recombinant Munc13-4 bound to purified Rab27A and Rab27B in their GTPγS-bound forms *in vitro*, indicating that their interaction is direct and nucleotide-dependent.

So far, eight proteins have been identified as GTP-Rab27A-binding molecules (43, 44). Five of them contain the C-terminal tandem calcium-binding C2 domains (45) and are designated as synaptotagmin-like proteins (Slp 1–5) (43, 44). The other three are homologous to Slps but lack the C2 domains and are designated as Slp-lacking C2 domains (Slac2-a–c) (43). All of these molecules contain the Slp homology domain at their N-terminal ends, through which these molecules interact directly with GTP-Rab27 (43). Munc13-4 does not contain this Slp homology domain motif (43, 44). Therefore, we conclude that Munc13-4 is a novel type of GTP-Rab27-binding molecule.

We have demonstrated that the addition of recombinant Munc13-4 in the secretion assay accelerated the kinetics and increased secretion, indicating that Munc13-4 positively regulates dense core granule secretion in platelets. Importantly, the inhibitory effect of unprenylated Rab27A was rescued by the addition of recombinant Munc13-4. Exogenously added unprenylated Rab27A is presumed to form nonfunctional complexes with putative Rab27 effectors, thereby inhibiting secretion. Because exogenously added Munc13-4 overcomes inhibition by unprenylated Rab27, it is most likely that Munc13-4 mediates the function of GTP-Rab27 in the dense core granule secretion in platelets. Interestingly, the inhibitory effect of unprenylated Rab27A on the secretion was stronger than that of unprenylated Rab27B (Fig. 1*A*), which may reflect distinct roles of each isoform within the regulation of dense core granule secretion in platelets. Our data suggest that this difference is due to the stronger affinity of Rab27A to Munc13-4 than that of Rab27B (Fig. 4*B*).

Because SNAREs and Rab GTPases are key molecules in the regulation of vesicle transport, elucidation of the molecular mechanism of their cooperation could provide a clue for further understanding of vesicle docking/fusion. There have been several examples of Rab effector proteins interacting with the components of the SNARE machinery. For example, the Rab5 effector Rabenosyn-5 interacts directly with Vps45, a member of the Munc18/Sec1 family, in the regulation of endocytic membrane traffic (46). Similarly, the Ypt7 effector complex that controls vacuolar fusion in yeast interacts directly with Vps33, which is also a Munc18/Sec1 family protein (47). Thus, a group of Rab effectors appear to regulate SNARE pairing through Munc18/Sec1 family proteins. Another group of Rab effectors has been shown to bind SNAREs directly, as shown for the Rab5 effector EEA1 interacting with syntaxin6 (48) and syntaxin13 (49).

It has also been demonstrated that Munc13-1 could be a direct regulator of syntaxin1 (50, 51) and that a GTP-Rab3A-binding protein, RIM1, which is a cytomatrix protein at the active zone in synapses, interacts with Munc13-1 (52). Thus, Rab3A might regulate Munc13-1 indirectly through interaction with RIM1. On the other hand, we here report the first direct link between Rab GTPases and a member of the Munc13 family, which may provide a novel mechanism for the control of SNARE activity by regulatory Rab GTPases. It will now be essential to explore the mechanisms of how Munc13-4 regulates the SNARE pairs that function in dense core granule secretion. In platelets, it has been shown that syntaxin2 mediates dense core granule secretion (53), suggesting that Munc13-4 might regulate syntaxin2.

We detected Munc13-4 in both cytosolic and membrane fractions, whereas Rab27 is exclusively in the membrane fraction (Fig. 5, *A* and *B*). Furthermore, by a density gradient separation, Munc13-4 was recovered in the plasma membrane fraction, whereas a major part of Rab27 was recovered in the granule fraction (Fig. 5*C*). Thus, the localization of Rab27 and Munc13-4 is not overlapping to a great extent. Munc13-4 on the plasma membrane may mark the target site for the dense core granule docking by interacting directly with activated Rab27 on the vesicle membrane. Because Rab3A is present on the synaptic vesicles (54) and its effector RIM1 and RIM1's partner Munc13-1 are on the presynaptic membrane in neurons (20), there might be a common regulatory mechanism used by the Rab GTPase-Munc13 system.

Taken together, the work presented here demonstrates that Rab27 regulates dense core granule secretion in platelets by employing the GTP-Rab27-binding protein, Munc13-4. Our current findings could provide a novel mechanism by which a Rab GTPase controls the regulated exocytosis through direct interaction with a Munc13 family protein. To contribute to further understanding of the regulation of vesicle transport, it is essential to elucidate the molecular mechanism of how the Rab27-Munc13-4 system promotes regulated exocytosis.

Acknowledgments—We are grateful to Dr. M. Zerial for providing plasmids containing Rab4 and Rab5, Dr. Y. Nozawa for a plasmid containing Rab27A, Dr. Y. Takai for a plasmid containing Rap1B and Rab3B, and Dr. K. Omori for providing an anti-Na,K-ATPase antibody. We are also grateful to the Kyoto Red Cross Blood Center for providing platelet pellets. We thank Dr. H. McBride (Ottawa, Canada) and Dr. C. Murphy (Ioannina, Greece) for critical reading of the manuscript and T. Matsubara for excellent technical assistance.

Note Added in Proof—Feldmann *et al.* (Feldmann, J., Callebaut, I., Raposo, G., Certain, S., Bacq, D., Dumont, C., Lambert, N., Ouachee-Chardin, M., Chedeville, G., Tamary, H., Minard-Colin, V., Vilmer, E., Blache, S., Le Deist, F., Fisher, A., and de Saint Basile, G. (2003) *Cell* **115**, 461–473) have published that mutation in Munc13-4 causes familial hemophagocytic lymphohistiocytosis (FHL3) where cytolytic granule fusion to the plasma membrane in cytotoxic T lymphocytes is impaired similar to mutation in Rab27A (11, 12), suggesting that the Rab27-Munc13-4 regulatory system may also function in regulated secretion in the cells.

REFERENCES

1. Brass, L. F. (2000) in *Hematology: Basic Principles and Practice* (Hoffman, R. S., Benz, E. J., Furie, B., Cohen, H., and Silberstein, L. E., ed) 3rd Ed., pp. 1753–1770, Churchill Livingston, New York
2. Takai, Y., Sasaki, T., and Matozaki, T. (2001) *Physiol. Rev.* **81**, 153–208
3. Zerial, M., and McBride, H. (2001) *Nat. Rev. Mol. Cell Biol.* **2**, 107–117
4. Wilson, S. M., Yip, R., Swing, D. A., O'Sullivan, T. N., Zhang, Y., Novak, E. K., Swank, R. T., Russell, L. B., Copeland, N. G., and Jenkins, N. A. (2000) *Proc. Natl. Acad. Sci. U. S. A.* **97**, 7933–7938
5. Wu, X. S., Rao, K., Zhang, H., Wang, F., Sellers, J. R., Matesic, L. E., Copeland, N. G., Jenkins, N. A., and Hammer, J. A., III (2002) *Nat. Cell Biol.* **4**, 271–278

6. Hume, A. N., Collinson, L. M., Hopkins, C. R., Strom, M., Barral, D. C., Bossi, G., Griffiths, G. M., and Seabra, M. C. (2002) *Traffic* **3,** 193–202
7. Provance, D. W., James, T. L., and Mercer, J. A. (2002) *Traffic* **3,** 124–132
8. Fukuda, M., Kuroda, T. S., and Mikoshiba, K. (2002) *J. Biol. Chem.* **277,** 12432–12436
9. Nagashima, K., Torii, S., Yi, Z., Igarashi, M., Okamoto, K., Takeuchi, T., and Izumi, T. (2002) *FEBS Lett.* **517,** 233–238
10. Kuroda, T. S., Ariga, H., and Fukuda, M. (2003) *Mol. Cell Biol.* **23,** 5245–5255
11. Stinchcombe, J. C., Bossi, G., Booth, S., and Griffiths, G. M. (2001) *Immunity* **15,** 751–761
12. Haddad, E. K., Wu, X., Hammer, J. A., III, and Henkart, P. A. (2001) *J. Cell Biol.* **152,** 835–842
13. Novak, E. K., Gautam, R., Reddington, M., Collinson, L. M., Copeland, N. G., Jenkins, N. A., McGarry, M. P., and Swank, R. T. (2002) *Blood* **100,** 128–135
14. Barral, D. C., Ramalho, J. S., Anders, R., Hume, A. N., Knapton, H. J., Tolmachova, T., Collinson, L. M., Goulding, D., Authi, K. S., and Seabra, M. C. (2002) *J. Clin. Invest.* **110,** 247–257
15. Chen, Y. A., and Scheller, R. H. (2001) *Nat. Rev. Mol. Cell Biol.* **2,** 98–106
16. Dulubova, I., Sugita, S., Hill, S., Hosaka, M., Fernandez, I., Sudhof, T. C., and Rizo, J. (1999) *EMBO J.* **18,** 4372–4382
17. Yang, B., Steegmaier, M., Gonzalez, L. C., Jr., and Scheller, R. H. (2000) *J. Cell Biol.* **148,** 247–252
18. Ashery, U., Varoqueaux, F., Voets, T., Betz, A., Thakur, P., Koch, H., Neher, E., Brose, N., and Rettig, J. (2000) *EMBO J.* **19,** 3586–3596
19. Richmond, J. E., Weimer, R. M., and Jorgensen, E. M. (2001) *Nature* **412,** 338–341
20. Brose, N., Hofmann, K., Hata, Y., and Sudhof, T. C. (1995) *J. Biol. Chem.* **270,** 25273–25280
21. Augustin, I., Betz, A., Herrmann, C., Jo, T., and Brose, N. (1999) *Biochem. J.* **337,** 363–371
22. Augustin, I., Rosenmund, C., Sudhof, T. C., and Brose, N. (1999) *Nature* **400,** 457–461
23. Varoqueaux, F., Sigler, A., Rhee, J. S., Brose, N., Enk, C., Reim, K., and Rosenmund, C. (2002) *Proc. Natl. Acad. Sci. U. S. A.* **99,** 9037–9042
24. Koch, H., Hofmann, K., and Brose, N. (2000) *Biochem. J.* **349,** 247–253
25. Akayama, M., Nakada, H., Omori, K., Masaki, R., Taketani, S., and Tashiro, Y. (1986) *Cell Struct. Funct.* **11,** 259–271
26. Palmer, M., Harris, R., Freytag, C., Kehoe, M., Tranum-Jensen, J., and Bhakdi, S. (1998) *EMBO J.* **17,** 1598–1605
27. Nagata, K., Satoh, T., Itoh, H., Kozasa, T., Okano, Y., Doi, T., Kaziro, Y., and Nozawa, Y. (1990) *FEBS Lett.* **275,** 29–32
28. Matsui, Y., Kikuchi, A., Kawata, M., Kondo, J., Teranishi, Y., and Takai, Y. (1990) *Biochem. Biophys. Res. Commun.* **166,** 1010–1016
29. Matsui, Y., Kikuchi, A., Kondo, J., Hishida, T., Teranishi, Y., and Takai, Y. (1988) *J. Biol. Chem.* **263,** 11071–11074
30. Chavrier, P., Vingron, M., Sander, C., Simons, K., and Zerial, M. (1990) *Mol. Cell Biol.* **10,** 6578–6585
31. Shirakawa, R., Yoshioka, A., Horiuchi, H., Nishioka, H., Tabuchi, A., and Kita, T. (2000) *J. Biol. Chem.* **275,** 33844–33849
32. Yoshioka, A., Shirakawa, R., Nishioka, H., Tabuchi, A., Higashi, T., Ozaki, H., Yamamoto, A., Kita, T., and Horiuchi, H. (2001) *J. Biol. Chem.* **276,** 39379–39385
33. Fabiato, A., and Fabiato, F. (1979) *J. Physiol. (Paris)* **75,** 463–505
34. Christoforidis, S., McBride, H. M., Burgoyne, R. D., and Zerial, M. (1999) *Nature* **397,** 621–625
35. Yoshioka, A., Horiuchi, H., Shirakawa, R., Nishioka, H., Tabuchi, A., Higashi, T., Yamamoto, A., and Kita, T. (2001) *Ann. N. Y. Acad. Sci.* **947,** 403–406
36. Knight, D. E., and Scrutton, M. C. (1980) *Thromb. Res.* **20,** 437–446
37. Nuoffer, C., Peter, F., and Balch, W. E. (1995) *Methods Enzymol.* **257,** 3–9
38. Pereira-Leal, J. B., Hume, A. N., and Seabra, M. C. (2001) *FEBS Lett.* **498,** 197–200
39. Franke, B., Akkerman, J. W., and Bos, J. L. (1997) *EMBO J.* **16,** 252–259
40. Menasche, G., Feldmann, J., Houdusse, A., Desaymard, C., Fischer, A., Goud, B., and de Saint Basile, G. (2003) *Blood* **101,** 2736–2742
41. Hume, A. N., Collinson, L. M., Rapak, A., Gomes, A. Q., Hopkins, C. R., and Seabra, M. C. (2001) *J. Cell Biol.* **152,** 795–808
42. Knight, J. B., Cao, K. T., Gibson, G. V., and Olson, A. L. (2000) *Endocrinology* **141,** 208–218
43. Kuroda, T. S., Fukuda, M., Ariga, H., and Mikoshiba, K. (2002) *J. Biol. Chem.* **277,** 9212–9218
44. Kuroda, T. S., Fukuda, M., Ariga, H., and Mikoshiba, K. (2002) *Biochem. Biophys. Res. Commun.* **293,** 899–906
45. Newton, A. C., and Johnson, J. E. (1998) *Biochim. Biophys. Acta* **1376,** 155–172
46. Nielsen, E., Christoforidis, S., Uttenweiler-Joseph, S., Miaczynska, M., Dewitte, F., Wilm, M., Hoflack, B., and Zerial, M. (2000) *J. Cell Biol.* **151,** 601–612
47. Price, A., Seals, D., Wickner, W., and Ungermann, C. (2000) *J. Cell Biol.* **148,** 1231–1238
48. Simonsen, A., Gaullier, J. M., D'Arrigo, A., and Stenmark, H. (1999) *J. Biol. Chem.* **274,** 28857–28860
49. McBride, H. M., Rybin, V., Murphy, C., Giner, A., Teasdale, R., and Zerial, M. (1999) *Cell* **98,** 377–386
50. Sassa, T., Harada, S., Ogawa, H., Rand, J. B., Maruyama, I. N., and Hosono, R. (1999) *J. Neurosci.* **19,** 4772–4777
51. Brose, N., Rosenmund, C., and Rettig, J. (2000) *Curr. Opin. Neurobiol.* **10,** 303–311
52. Schoch, S., Castillo, P. E., Jo, T., Mukherjee, K., Geppert, M., Wang, Y., Schmitz, F., Malenka, R. C., and Sudhof, T. C. (2002) *Nature* **415,** 321–326
53. Chen, D., Bernstein, A. M., Lemons, P. P., and Whiteheart, S. W. (2000) *Blood* **95,** 921–929
54. Matteoli, M., Takei, K., Cameron, R., Hurlbut, P., Johnston, P. A., Sudhof, T. C., Jahn, R., and De Camilli, P. (1991) *J. Cell Biol.* **115,** 625–633

Role of Bone Marrow–Derived Progenitor Cells in Cuff-Induced Vascular Injury in Mice

Yang Xu, Hidenori Arai, Xin Zhuge, Hideto Sano, Toshinori Murayama, Momoko Yoshimoto, Toshio Heike, Tatsutoshi Nakahata, Shin-ichi Nishikawa, Toru Kita, Masayuki Yokode

Objectives—Arterial injury results in vascular remodeling associated with proliferation and migration of smooth muscle cells (SMCs) and the development of intimal hyperplasia, which is a critical component of restenosis after angioplasty of human coronary arteries and an important feature of atherosclerotic lesions. However, the origin of SMCs and other cells in the development of vascular remodeling is not yet fully understood.

Methods and Results—We utilized a cuff-induced vascular injury model after transplantation of the bone marrow (BM) from green fluorescent protein (GFP)-transgenic mice. We found that macrophages were major cells recruited to the adventitia of the vascular injury lesion along with SMCs and endothelial cells (ECs). While investigating whether those cells are derived from the donor, we found that most of the macrophages were GFP-positive, and some of the SMCs and ECs were also GFP-positive. Administration of the anti–c-*fms* antibody resulted in a marked decrease in macrophages and a relative increase of SMCs, while administration of antibodies against the platelet-derived growth factor receptor-β caused a prominent decrease in SMCs and a relative increase in macrophages.

Conclusions—The current study indicates that BM-derived cells play an important role in vascular injury, and that differentiation of macrophages and SMCs might be dependent on each other. (***Arterioscler Thromb Vasc Biol.* 2004; 24:477-482.)**

Key Words: macrophage ■ smooth muscle cell ■ endothelial cell ■ vascular injury ■ bone marrow

Arterial injury results in proliferation and migration of smooth muscle cells (SMCs) and the development of intimal hyperplasia, a critical component of restenosis after angioplasty of human coronary arteries and an important feature of atherosclerotic lesions. However, the origin of SMCs, which engage in the development of neointimal thickening during vascular disease, is not yet fully understood. One possibility is that medial SMCs are phenotypically modified and migrate into the intima, where they proliferate and secrete extracellular matrix components.[1] It has also been proposed that adventitial fibroblasts move into the neointima and give rise to cells with smooth-muscle–like properties.[2]

Recently, several groups have reported that cells of recipient origin take part in the formation of neointimal SMCs during the development of transplant vasculopathy.[3–5] These results agree with the notion that adult bone marrow (BM) contains multipotent cells that can develop into various lineages.[6] It has also been shown that endothelial progenitor cells (EPCs) can transdifferentiate into SMCs.[7] Thus, the origin of SMCs in atherosclerotic lesions is a source of controversy, and it is important to understand the contribution of BM-derived cells to neointimal formation in vascular pathology.

In vascular injury or remodeling, it is not clear whether one specific type of multipotent precursor cell can differentiate into endothelial cells (ECs), SMCs, or macrophages, or whether there are different precursor cells for each cell lineage. We have reported that administration of anti–c-*fms* antibody can prevent early atherosclerosis in apolipoprotein E-deficient (apoE$^{-/-}$) mice.[8] We have also shown that administration of antibodies against the platelet-derived growth factor receptor-β (anti–PDGFR-β) can prevent the recruitment of SMCs, but not of macrophages in the atherosclerotic lesions in apoE$^{-/-}$ mice.[9] These results indicate the important role of macrophages in the initiation of the lesion and recruitment of SMCs in hyperlipidemia-induced atherosclerosis. However, it is not known whether the recruitment of macrophages is critical for the migration of SMCs in vascular injury.

Therefore, we have two goals in this study. One is to explore the contribution of BM-derived cells to the development of vascular remodeling. The other is to examine whether blocking the cell differentiation by a specific antibody can affect the lesion formation in vascular injury. For this purpose we have utilized an inflammation-dependent vascular disease

Received November 16, 2003; revision accepted January 5, 2004.

From the Departments of Geriatric Medicine (H.S.), Pediatrics (M. Yoshimoto, T.H., T.N.), and Cardiovascular Medicine (T.K.), Kyoto University Graduate School of Medicine, Japan; the Translational Research Center (Y.X., X.Z., T.M., M. Yokode), Kyoto University Hospital, Kyoto, Japan; and the RIKEN Center for Developmental Biology (S.N.), Kobe, Japan

Correspondence to Hidenori Arai, MD, PhD, Department of Geriatric Medicine, Kyoto University Graduate School of Medicine, 54 Kawahara-cho, Shogoin, Sakyo-ku, Kyoto, 606-8507, Japan. E-mail harai@kuhp.kyoto-u.ac.jp

Arterioscler Thromb Vasc Biol. is available at http://www.atvbaha.org DOI: 10.1161/01.ATV.0000118016.94368.35

model induced by polyethylene cuff placement around the femoral artery after BM transplantation (BMT) from green fluorescent protein (GFP)-transgenic mice.

Methods

Mice

All experimental protocols were performed in accordance with the guidelines of Kyoto University, Japan. GFP-transgenic mice with C57BL/6 background were a generous gift from Dr. M. Okabe[10] (Osaka University, Japan). The mice were kept in a temperature-controlled facility on a 14-hour light/10-hour dark cycle, with free access to food and water. Mice were fed a normal chow diet containing 8.7% (wt/wt) fat and 0.063% (wt/wt) cholesterol (Oriental Yeast, Chiba, Japan) for the entire period of the experiment.

Bone Marrow Transplantation

Femurs of male or female, 8- to 12-week-old GFP-transgenic mice were dissected, and surrounding muscle tissue was removed by microscissors. Bones were then left in Dulbecco's modified Eagle's medium (DMEM). Both ends of the bones were cut with scissors, and the marrow was flushed with DMEM using a syringe with a 21-gauge needle. The marrow clusters were disaggregated by vigorous pipetting. BM cells were washed, resuspended in PBS, and counted. Eight-week-old female C57BL/6 mice were subjected to a lethal dose of total body irradiation (9 Gy) using the Gammacell 40 Exactor Irradiator (Nordion International). Each irradiated recipient received 5×10^5 BM cells extracted from GFP-transgenic mice in 0.5 mL PBS by tail vein injection. Mice used for BMT experiments were housed in sterilized cages and fed sterilized normal chow diet. Drinking water was supplied with 0.1% hydrochloric acid. Four weeks after BMT, the recipient mice were phlebotomized, and the circulating leukocytes were then checked for the expression of GFP by flow cytometry. Cuff placement was performed at least 4 weeks after BMT.

Cuff Placement

Mice were anesthetized with barbiturate complex [propylene glycol 17.9% (v/v), ethanol 8.9% (v/v), sodium 5-ethyl-5-(1-methylbutyl) barbiturate 10.7% (v/v)]. The right femoral artery was dissected from its surroundings. A nonconstrictive polyethylene cuff (PE50, 0.58 mm inner diameter, 0.965 mm outer diameter, 2 mm length; Becton Dickinson) was placed loosely around the right femoral artery.

Antibody Administration

AFS98, a rat monoclonal anti-murine c-*fms* antibody, which inhibits colony formation dependent on macrophage-colony stimulating factor (M-CSF) and cell growth by blocking the binding of M-CSF to its receptor c-*fms*, was previously described as an anti-c-*fms* antibody.[9] APB5, a rat monoclonal anti-murine PDGFR-β antibody, which blocks the PDGFR-β–mediated signaling pathway, was also described.[9] Four C57BL/6 mice in each group were administered 1 mg of AFS98, APB5, or isotype-matched irrelevant rat IgG (γ2A) once a day for 2 weeks after cuff placement.

Tissue Preparation

At euthanization, mice were anesthetized with barbiturate complex. Mouse thorax was opened, and physiological pressure-perfusion-fixation (100 mm Hg) was performed by cardiac puncture with 4% paraformaldehyde in PBS for 10 minutes. After the procedures, bilateral femoral arteries were harvested. The tissue was snap-frozen in OCT compound (Sakura Finetek). Serial cross sections (6 μm thick) were obtained throughout the entire length of the cuffed femoral artery or equivalent portion of the contralateral artery for histological analysis. Rat monoclonal antibody (mAb) BM8, labeled with biotin (BMA Biochemicals AG), was used as a specific marker for mouse macrophages. For macrophage staining, we used the Tyramide Signal Amplification system (NEN Life Science Products) to amplify the weak signal. For SMC staining, we used mouse monoclonal anti-human smooth muscle α-actin (SMA) antibody (clone 1A4), labeled with Cy3 (Sigma). For the staining of smooth muscle myosin heavy chain SM1,[11] we used rat anti-SM1 mAb (clone KM995) (kindly provided by the Kyowa Hakko Kogyo Co, Tokyo, Japan). Sections were secondarily incubated with rhodamine-labeled anti-rat IgG (Chemicon). ECs were identified by immunohistochemical staining with biotin-conjugated rat anti-mouse CD31 antibody (Southern Biotech) and rabbit anti-von Willebrand Factor (vWF) antibody (Sigma). For CD31 staining, the Tyramide Signal Amplification system was employed to augment antigenicity of ECs. For vWF staining, sections were secondarily incubated with rhodamine-labeled anti-rabbit IgG (Chemicon).

Image Analysis and Quantification

Eight equally crossed sections were used from each mouse to quantify the femoral artery lumen, BM-derived cell area, and vascular remodeling lesion size. Sections were evaluated by using Image-Pro Plus (Media Cybernetics). To estimate the effect of anti-c-*fms* or anti-PDGFR-β on vascular remodeling, we calculated the ratio of the number of SMCs or macrophages to the whole vascular remodeling lesion area. The area of the femoral artery lumen, BM-derived cells, and vascular remodeling lesion was calculated and expressed in square micrometers.

Statistical Analysis

Data are expressed as mean±SEM and were analyzed by ANOVA with Abacus Statview software (version 5.0). A value of $P<0.05$ was regarded as significant.

Results

Recruitment of Bone Marrow–Derived Progenitor Cells in Cuff-Induced Vascular Remodeling

To elucidate the involvement of BM-derived cells in cuff-induced vascular remodeling lesions, BM cells from GFP-transgenic mice were transplanted into lethally irradiated C57BL/6 mice before cuff placement. After 4 weeks of BMT, we confirmed the reconstitution of the hematopoietic system by checking the fluorescence of blood leukocytes by flow cytometry. We found that more than 85% of the cells were positive for GFP (data not shown); this finding indicates that most of the leukocytes were derived from the donor BM. One or two weeks after cuff placement, cuffed or sham-operated femoral arteries were examined under fluorescence microscopy. In the cuffed artery, the majority of the cells accumulating in the lesion were GFP-positive (Figure 1A and 1B), suggesting that those cells were derived from the donor BM. In contrast, in the sham-operated artery, GFP-positive cells were hardly detected (Figure 1C). We found that the accumulation of BM-derived cells in the vascular remodeling lesion was significantly increased from 1 week to 2 weeks after cuff placement (Figure 1A, 1B, and 1D). Although we did not find a visible change in intimal thickening after cuff placement, the lumen of the cuffed artery was more restricted than that of the sham-operated artery (Figure 1E).

Macrophages are the Major Component in the Cuff-Induced Vascular Remodeling Lesion

Next, to examine the recruitment of macrophages in the cuffed lesion, we stained the tissue with BM8. We found many cells recruited to the adventitia of the cuffed artery, most of which were positive for BM8 (Figure 2A), indicating the role of monocyte-macrophages in vascular remodeling

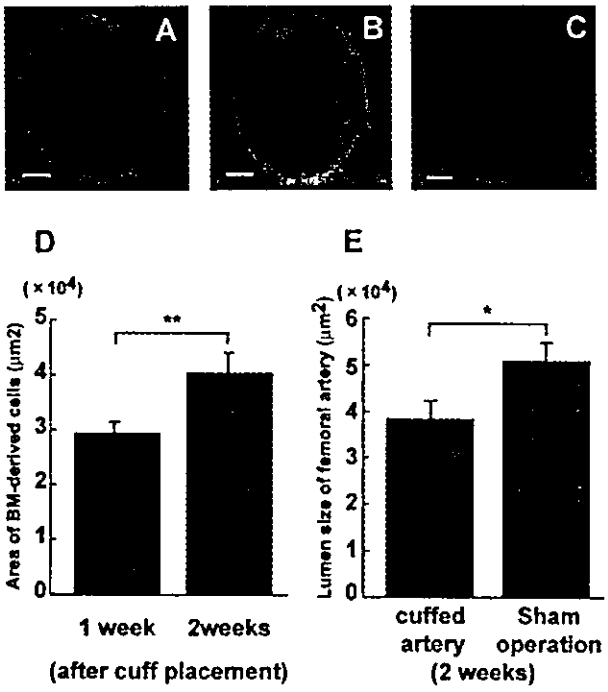

Figure 1. A through C, Representative microscopic photographs of BM-derived GFP-positive cells in C57BL/6 mouse vascular remodeling lesion. Four weeks after BMT, a nonconstrictive polyethylene cuff was placed around the right femoral artery in four mice in each group. The cuffed (A, 1 week after cuff placement; B, 2 weeks after cuff placement) or sham-operated (C) femoral arteries were examined under fluorescence microscopy. D and E, Quantitative analyses of BM-derived cell area (D) and femoral artery lumen area (E) after cuff placement showed a significant difference between 2 groups. Data from 20 slices per mouse artery are shown as mean±SEM. $^{*}P<0.05$, $^{**}P<0.01$. Scale bars: 100 μm

lesions. In the sham-operated femoral artery, we found few BM8-positive cells (Figure 2B).

BM Cells Can Differentiate into Vascular Smooth Muscle Cells

To examine whether BM-derived cells can differentiate into SMCs in the vascular remodeling lesion, we stained the tissue with Cy3-labeled anti-SMA (clone 1A4) and anti-SM1 (clone

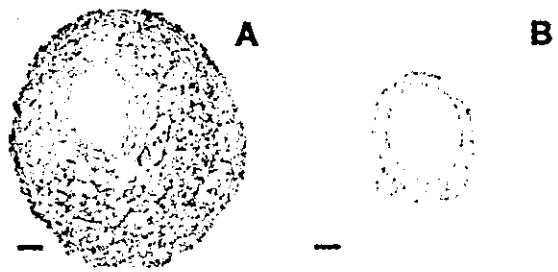

Figure 2. Numerous macrophage-like cells accumulating in the cuff-induced vascular remodeling lesion. After 2 weeks of cuff placement as described in Figure 1, tissues were subjected to immunohistochemistry with biotinylated anti-mouse macrophage antibody BM8. A number of cells were BM8-positive cells in cuffed femoral artery (A), but in the sham operated femoral artery, those cells could hardly be found (B). Scale bars: 100 μm

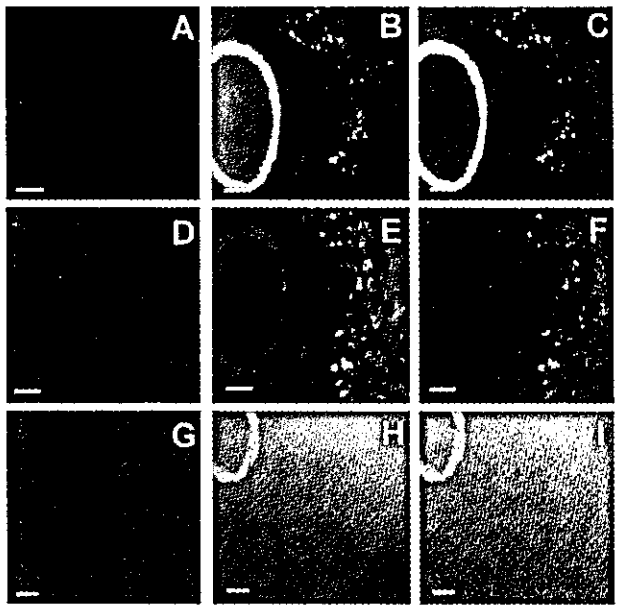

Figure 3. BM-derived SMCs in C57BL/6 mouse vascular remodeling lesion. After the same procedure in Figure 1, tissues were subjected to immunohistochemistry with antibodies to Cy3-labeled SMA (B, H) or SM1 (E). A, D, and G are fluorescent microscopic photographs for GFP. G, H, and I are fluorescent microscopic photographs from femoral artery of 1 week after cuff placement. All the others are samples at 2 weeks after cuff placement. C, F, and I are merged images of GFP and Cy3 signal from A and B, D and E, and G and H, respectively. Scale bars: 100 μm

KM995) antibodies. We found a number of 1A4- and KM995-positive cells in the adventitia of the lesion (Figure 3B and 3E). With the colorization of GFP signals, we observed that some of the 1A4- and KM995-positive cells were also positive for GFP (Figure 3C and 3F), indicating that BM-derived cells can also differentiate to SMCs in the cuff-induced vascular remodeling lesion. However, in the earlier time point at 1 week after cuff placement, we could find few SMCs in vascular remodeling lesion (Figure 3H).

Interference Exists Between Macrophages and Smooth Muscle Cells

To examine whether inhibiting the differentiation to macrophage or SMC by mAb could affect the manner of accumulation and differentiation of BM-derived cells in the vascular remodeling lesion, we administered an antagonistic rat mAb against murine c-*fms* (M-CSF receptor) (clone AFS98) or PDGFR-β (clone APB5) to C57BL/6 female mice which had undergone cuff placement. In comparison with the lesion from mice administered with control IgG (clone γ2A) (Figure 4C), we found that the treatment with AFS98 caused a marked decrease in macrophages in the lesion (Figure 4A and 4G). Interestingly, the density of SMCs was inversely increased (Figure 4D and 4H) in response to this treatment. In contrast, administration of APB5 resulted in a marked increase in macrophages (Figure 4B and 4G) with a concomitant decrease of SMCs (Figure 4E and 4H), suggesting that a certain interaction occurs between macrophages and SMCs during the vascular remodeling process.

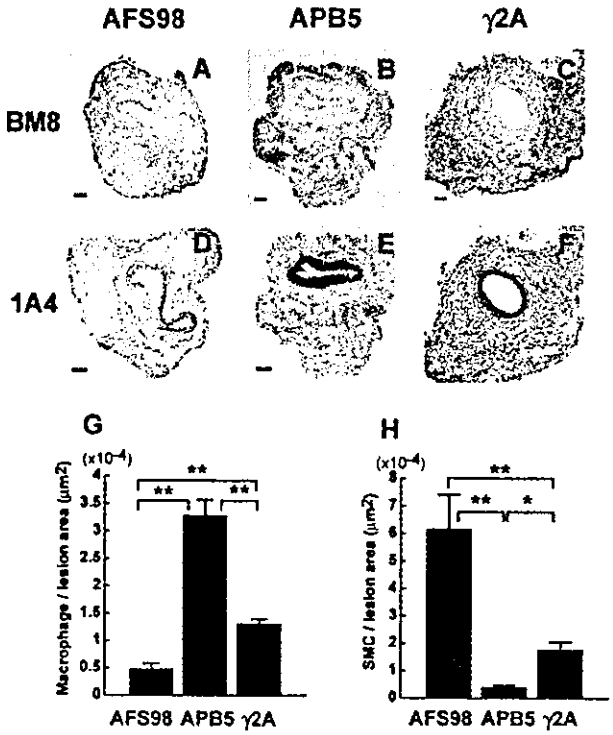

Figure 4. Progenitors of SMC and macrophage have opposite roles in the lesion formation. A total of 12 C57BL/6 mice (8 weeks of age) were injected for 2 weeks with 1 mg of AFS98 (n=4), APB5 (n=4), or γ2A (n=4) every day after cuff placement. Each mouse was euthanized and the femoral artery was subjected to immunohistochemistry with anti-macrophage antibody (A, B, and C) or anti-SMA antibody (D, E, and F). A and D are from mice injected with AFS98, B and E are from mice injected with APB5, and C and F are from mice given γ2A. Ratio of the number of macrophages (G) and SMCs (H) to whole vascular remodeling lesion area had a significant difference in each group. Data from 20 slices per mouse are shown as mean±SEM. *$P<0.05$, **$P<0.01$. Scale bars: 100 μm

To estimate the effects of anti–PDGFR-β or anti–c-*fms* mAb on vascular remodeling, we measured the lumen size of the artery treated with the two kinds of mAb and γ2A. We found no distinct difference in the lumen size of the femoral artery through administration of AFS98, APB5, or γ2A (data not shown).

We also examined whether each antibody administration had any effect on tissue formation after cuff placement. The calculated vascular remodeling lesion area of each mouse treated with AFS98, APB5, and γ2A was $1.18\times10^5\pm5.38\times10^3$ μm², $1.43\times10^5\pm7.27\times10^3$ μm², and $1.82\times10^5\pm1.11\times10^4$ μm², respectively (mean±SEM of 20 slices from each of 4 mice, $P<0.05$ versus γ2A). Less tissue formation was observed in the mice treated with AFS98 and APB5 than in mice treated with γ2A. This result indicates that AFS98 and APB5 administration could inhibit tissue formation after cuff placement. Further, to examine whether APB5 or AFS98 has an effect on BM-derived cell incorporation, we performed cuff placement and administered each antibody to mice that had been subjected to BMT. By measuring BM-derived cells accumulating in the cuff-induced lesion, we found a significant decrease of GFP-positive cells by mAb administration (data not shown), indicating that APB5 and AFS98 also affected the incorporation of BM-derived cells.

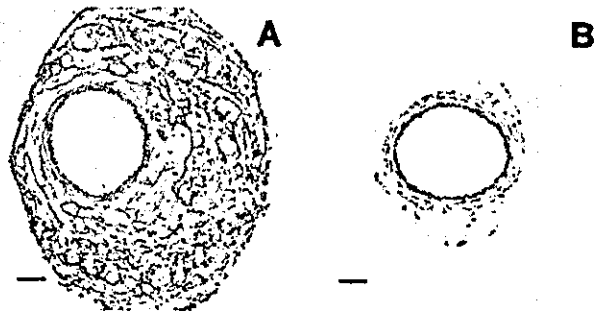

Figure 5. Representative microscopic photographs of BM-derived ECs in cuff-induced vascular remodeling lesion. After the same procedure in Figure 1, tissues were subjected to immunohistochemistry with biotin-conjugated rat anti-mouse CD31. The microscopic photograph of A is from cuffed right femoral artery, and B is from sham-operated left femoral artery. Scale bars: 100 μm

Endothelial Progenitor Cells Are Recruited to the Cuffed Vascular Remodeling Lesion

Because it is not known whether EPCs can contribute to cuff-induced vascular remodeling lesion formation in the injured femoral artery, we performed a series of endothelial staining. We found that the endothelial lining of the intima was clearly stained with anti-CD31 antibody, and that small vessels in the adventitia were also stained. There were also some CD31-positive cells clustered outside the small vessels in the adventitia in the cuffed lesions (Figure 5A), but not in the sham-operated lesions (Figure 5B). Because CD31 can also be expressed on monocyte-macrophages, we stained the tissue with anti-vWF antibody, another EC-specific marker, and compared the expression with GFP-positive cells. As shown in Figure 6E, the endothelial lining of the intima and small vessels in the adventitia were also positive for vWF. Some of the clustered cells in the adventitia were positive for

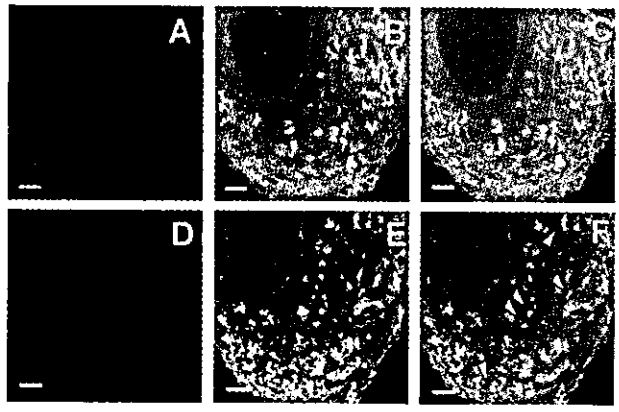

Figure 6. EPCs in cuff-induced vascular remodeling lesions. After the same procedure in Figure 1, tissues were subjected to immunostaining with anti-vWF antibody. A, B, and C are 1 week after cuff placement, and D, E, and F are 2 weeks after cuff placement. A and D indicate GFP signals, and B and E indicate vWF signals. C is a merged image of A and B, and F is a merged image of D and E. Scale bars: 100 μm

vWF and GFP, while the endothelial lining of the intima of the artery and small vessels in the adventitia were only positive for vWF (Figure 6F), indicating the involvement of angiogenesis from vasa vasorum. Notably, as we observed that significantly fewer SMCs could be found 1 week after cuffing (Figure 3B), EPCs could scarcely be found in the vascular remodeling lesion at this earlier phase (Figure 6C).

Discussion

In this study, we have clearly shown that BM-derived cells are critically involved in the lesion formation of cuff-induced vascular remodeling in mice. In this setting, BM-derived macrophages, SMCs, and ECs contributed to the lesion formation. However, not all of the SMCs or ECs in the lesion were derived from the BM. Interestingly, when anti–c-*fms* antibody was administered after cuff placement, the recruitment of macrophages was suppressed, but the density of SMCs was increased. On the other hand, administration of anti–PDGFR-β inhibited the recruitment of SMCs in the vascular remodeling lesion, but increased the number of macrophages. These results suggest an interaction between macrophages and SMCs during the lesion formation.

Although previous investigators have shown intimal thickening in the cuff-induced vascular injury model,[12,13] we have not been able to reproduce their results. This may be due to the technique of the cuff placement, because we were able to induce intimal thickening of the cuffed artery when we used apoE$^{-/-}$ mice fed with high-fat diet (data not shown). Indeed, we found a marked inflammatory change in the adventitial region around the cuffed artery. However, little is known about inflammatory responses in the adventitia after vascular injury, and adventitial and perivascular reactions are largely ignored. Recent clinical and experimental data by other investigators suggest that constrictive vascular remodeling is in large part responsible for lumen loss associated with restenosis.[14,15] Scott et al have indicated that the adventitia may be important in the first wave of growth after angioplasty of coronary arteries, with later growth of the lesion occurring in the neointima.[16] Therefore, studying the mechanism of cell recruitment to the adventitia in the vascular remodeling region is important for the understanding of the pathogenesis of restenosis.

Recent studies for transplant atherosclerosis have demonstrated that most of the neointimal α-actin–positive SMCs in recipient coronary arteries or aortas were from host origin,[4,5] suggesting that these SMCs might be at least in part from BM-derived smooth muscle progenitor cells. In this study, we have demonstrated that at least three types of cells, macrophage, SMC, and EC, are recruited from the BM to the adventitia of the cuff-induced vascular injury site. The characteristic feature of those cells is to form a cluster in the lesion. However, we have not determined when and how those cells migrate to the adventitia. Therefore, it is very important to understand the timing and pathway of cell migration in the pathogenesis of vascular injury. Elucidating the involvement of soluble factors in this model, such as chemokines and adhesion molecules, would also be intriguing.

In this study we have shown that administration of anti–c-*fms* antibody inhibited the recruitment of macrophages, and increased the recruitment of SMCs to the vascular injury lesion in wild-type mice. This finding is different from our report on apoE$^{-/-}$ mice, where we showed that the antibody inhibited the recruitment of SMCs as well as macrophages in early atherosclerotic lesion.[8] Thus, in hyperlipidemia-induced atherosclerosis, the recruitment of monocyte-macrophage is prerequisite for the migration of SMCs for the lesion formation; this paradigm was not applied to the current vascular injury model. If the common progenitors for macrophage and SMC exist, our data might indicate that BM-derived cells are playing an important role in vascular injury, but not in hyperlipidemia-induced atherosclerosis. The result with anti–PDGFR-β is also different from our previous observation in apoE$^{-/-}$ mice,[9] in which the antibody to apoE$^{-/-}$ mice failed to affect the density of macrophages in advanced atheromatous lesions. It was also notable that administration of anti–PDGFR-β increased the recruitment of macrophages in this study. Thus, in the vascular injury model, blocking the differentiation of one cell type can increase the recruitment or differentiation of the other cell type. Although we have not determined whether the progenitors of macrophages and SMCs are derived from the same precursor cell, anti–c-*fms* or anti–PDGFR-β might affect the differentiation of common precursor cells.

Schmeisser et al reported that BM-derived macrophages might contribute to neovascularization by in situ transdifferentiation to EC-like cells.[17] We found that in the vascular injury lesion there were many cells positive for CD31, which is an endothelial marker and is also positive for monocyte-lineage. However, vWF-positive cells were much smaller in number in this lesion. Furthermore, most of the cells forming a small vessel were positive for vWF, but negative for GFP, indicating that the source of the ECs forming a small vessel in the adventitia is from vasa vasorum, not from the BM.

Terada et al[18] and Ying et al[19] demonstrated that embryonic stem cells can spontaneously fuse with mononuclear BM cells[18] or brain cells[19] in vitro to form pluripotent tetraploid hybrids. In this study, there are a number of BM-derived cells stimulated after cuff placement in the cuff-induced vascular remodeling lesion. These BM-derived cells play an important role for lesion formation. Those two reports showed that the frequency of cell fusion was very low (2×10^{-6} to 10^{-4}), although it is difficult to directly correlate the in vitro findings of embryonic stem cells to our in vivo study. It is possible that some of the BM-derived cells in our experiments resulted from fusion between BM cells and vascular cells; however, this phenomenon would be an unlikely explanation for the extent of BM involvement seen in this study.

In summary, we have provided evidence that BM-derived cells are playing a critical role in cuff-induced vascular injury in mice. Understanding the interaction among the cells involved in the lesion formation will be important for regulating the accumulation of inflammatory cells in the vascular injury lesion.

Acknowledgments

This study was supported by Grants-in-Aid from the Ministry of Education, Science, Sports, and Culture of Japan (20045982, 12671111, 14571093, and 13307034) (to H.A.. M.Y., T.K.); Center of Excellence grants (12CE2006) (to T.K.); a research grant for health sciences from the Japanese Ministry of Health and Welfare (to T.K.); and a grant from the Rotary Yoneyama Memorial Foundation (to Y.X.). T.M. is supported by Establishment of International COE for Integration of Transplantation Therapy and Regenerative Medicine (COE Program of the Ministry of Education, Culture, Sports, Science, and Technology, Japan). We thank Drs Hiroharu Kataoka and Masafumi Morimoto for their advice about cuff placement, and Akiko Kato for her excellent technical assistance.

References

1. Newby AC, Zaltsman AB. Molecular mechanisms in intimal hyperplasia. *J Pathol.* 2000;190:300–309.
2. Zalewski A, Shi Y. Vascular myofibroblasts. Lessons from coronary repair and remodeling. *Arterioscler Thromb Vasc Biol.* 1997;17:417–422.
3. Plissonnier D, Nochy D, Poncet P, Mandet C, Hinglais N, Bariety J, Michel JB. Sequential immunological targeting of chronic experimental arterial allograft. *Transplantation.* 1995;60:414–424.
4. Hillebrands JL, Klatter FA, van den Hurk BM, Popa ER, Nieuwenhuis P, Rozing J. Origin of neointimal endothelium and α-actin–positive smooth muscle cells in transplant arteriosclerosis. *J Clin Invest.* 2001;107: 1411–1422.
5. Saiura A, Sata M, Hirata Y, Nagai R, Makuuchi M. Circulating smooth muscle progenitor cells contribute to atherosclerosis. *Nat Med.* 2001;7: 382–383.
6. Pittenger MF, Mackay AM, Beck SC, Jaiswal RK, Douglas R, Mosca JD, Moorman MA, Simonetti DW, Craig S, Marshak DR. Multilineage potential of adult human mesenchymal stem cells. *Science.* 1999;284: 143–147.
7. DeRuiter MC, Poelmann RE, VanMunsteren JC, Mironov V, Markwald RR, Gittenberger-de Groot AC. Embryonic endothelial cells transdifferentiate into mesenchymal cells expressing smooth muscle actins in vivo and in vitro. *Circ Res.* 1997;80:444–451.
8. Murayama T, Yokode M, Kataoka H, Imabayashi T, Yoshida H, Sano H, Nishikawa S, Kita T. Intraperitoneal administration of anti–c-*fms* monoclonal antibody prevents initial events of atherogenesis but does not reduce the size of advanced lesions in apolipoprotein E-deficient mice. *Circulation.* 1999;99:1740–1746.
9. Sano H, Sudo T, Yokode M, Murayama T, Kataoka H, Takakura N, Nishikawa S, Nishikawa SI, Kita T. Functional blockade of platelet-derived growth factor receptor-β but not of receptor-α prevents vascular smooth muscle cell accumulation in fibrous cap lesions in apolipoprotein E-deficient mice. *Circulation.* 2001;103:2955–2960.
10. Okabe M, Ikawa M, Kominami K, Nakanishi T, Nishimune Y. 'Green mice' as a source of ubiquitous green cells. *FEBS Lett.* 1997;407: 313–319.
11. Nagai R, Kuro-o M, Babij P, Periasamy M. Identification of two types of smooth muscle myosin heavy chain isoforms by cDNA cloning and immunoblot analysis. *J Biol Chem.* 1989;264:9734–9737.
12. Liu HW, Iwai M, Takeda-Matsubara Y, Wu L, Li JM, Okumura M, Cui TX, Horiuchi M. Effect of estrogen and AT1 receptor blocker on neointima formation. *Hypertension.* 2002;40:451–457; discussion 448–450.
13. Suzuki J, Iwai M, Nakagami H, Wu L, Chen R, Sugaya T, Hamada M, Hiwada K, Horiuchi M. Role of angiotensin II-regulated apoptosis through distinct AT1 and AT2 receptors in neointimal formation. *Circulation.* 2002;106:847–853.
14. Mintz GS, Popma JJ, Pichard AD, Kent KM, Satler LF, Wong C, Hong MK, Kovach JA, Leon MB. Arterial remodeling after coronary angioplasty: a serial intravascular ultrasound study. *Circulation.* 1996;94: 35–43.
15. Sangiorgi G, Taylor AJ, Farb A, Carter AJ, Edwards WD, Holmes DR, Schwartz RS, Virmani R. Histopathology of postpercutaneous transluminal coronary angioplasty remodeling in human coronary arteries. *Am Heart J.* 1999;138:681–687.
16. Scott NA, Cipolla GD, Ross CE, Dunn B, Martin FH, Simonet L, Wilcox JN. Identification of a potential role for the adventitia in vascular lesion formation after balloon overstretch injury of porcine coronary arteries. *Circulation.* 1996;93:2178–2187.
17. Schmeisser A, Garlichs CD, Zhang H, Eskafi S, Graffy C, Ludwig J, Strasser RH, Daniel WG. Monocytes coexpress endothelial and macrophagocytic lineage markers and form cord-like structures in Matrigel under angiogenic conditions. *Cardiovasc Res.* 2001;49:671–680.
18. Terada N, Hamazaki T, Oka M, Hoki M, Mastalerz DM, Nakano Y, Meyer EM, Morel L, Petersen BE, Scott EW. Bone marrow cells adopt the phenotype of other cells by spontaneous cell fusion. *Nature.* 2002; 416:542–545.
19. Ying QL, Nichols J, Evans EP, Smith AG. Changing potency by spontaneous fusion. *Nature.* 2002;416:545–548.

Cell surface-anchored SR-PSOX/CXC chemokine ligand 16 mediates firm adhesion of CXC chemokine receptor 6-expressing cells

Takeshi Shimaoka,* Takashi Nakayama,† Noriko Fukumoto,* Noriaki Kume,‡ Shu Takahashi,§ Junko Yamaguchi,§ Manabu Minami,‡ Kazutaka Hayashida,‡ Toru Kita,‡ Jun Ohsumi,¶ Osamu Yoshie,† and Shin Yonehara*,[1]

*Graduate School of Biostudies and Institute for Virus Research and ‡Department of Cardiovascular Medicine, Graduate School of Medicine, Kyoto University, Sakyo-ku, Japan; †Department of Microbiology, Kinki University School of Medicine, Osaka-Sayama, Japan; and §Biomedical Research Laboratories and ¶Molecular Biology Research Laboratories, Sankyo Co. Ltd., Shinagawa-ku, Tokyo, Japan

Abstract: Direct contacts between dendritic cells (DCs) and T cells or natural killer T (NKT) cells play important roles in primary and secondary immune responses. SR-PSOX/CXC chemokine ligand 16 (CXCL16), which is selectively expressed on DCs and macrophages, is a scavenger receptor for oxidized low-density lipoprotein and also the chemokine ligand for a G protein-coupled receptor CXC chemokine receptor 6 (CXCR6), expressed on activated T cells and NKT cells. SR-PSOX/CXCL16 is the second transmembrane-type chemokine with a chemokine domain fused to a mucin-like stalk, a structure very similar to that of fractalkine (FNK). Here, we demonstrate that SR-PSOX/CXCL16 functions as a cell adhesion molecule for cells expressing CXCR6 in the same manner that FNK functions as a cell adhesion molecule for cells expressing CX_3C chemokine receptor 1 (CX_3CR1) without requiring CX_3CR1-mediated signal transduction or integrin activation. The chemokine domain of SR-PSOX/CXCL16 mediated the adhesion of CXCR6-expressing cells, which was not impaired by treatment with pertussis toxin, a Gαi protein blocker, which inhibited chemotaxis of CXCR6-expressing cells induced by SR-PSOX/CXCL16. Furthermore, the adhesion activity was up-regulated by treatment of SR-PSOX/CXCL16-expressing cells with a metalloprotease inhibitor, which increased surface expression levels of SR-PSOX/CXCL16. Thus, SR-PSOX/CXCL16 is a unique molecule that not only attracts T cells and NKT cells toward DCs but also supports their firm adhesion to DCs. *J. Leukoc. Biol.* 75: 267–274; 2004.

Key Words: *scavenger receptor · metalloprotease · T cells*

INTRODUCTION

The chemokine superfamily consists of small, heparin-binding cytokines that induce directed migration of various types of leukocytes through interactions with a group of seven-transmembrane G protein-coupled receptors [1]. More than 40 chemokines have been identified and classified into four subfamilies, C, CC, CXC, and CX_3C, based on the motif formed by the conserved cysteine residues in the amino-terminal region. In addition to migration-inducing activity, chemokines have been shown to induce signals that lead to cytoskeletal reorganization and integrin activation for cell adhesion [2–5]. Furthermore, fractalkine (FNK)/CX_3C chemokine ligand 1, the first reported transmembrane-type chemokine [6, 7], has been shown to function as a cell adhesion molecule under static and flow conditions without requiring CX_3C chemokine receptor 1 (CX_3CR1)-mediated signaling or integrin activation [8, 9].

Recently, we have identified and characterized SR-PSOX, a novel scavenger receptor for phosphatidylserine and oxidized low-density lipoprotein and bacteria [10, 11]. Separately, other groups have identified chemokine ligand 16 (CXCL16) [12, 13], the chemokine ligand for a G protein-coupled receptor CXC chemokine receptor 6 (CXCR6) [14, 15], and then SR-PSOX and CXCL16 turned out to be identical. Thus, SR-PSOX/CXCL16 is the second transmembrane-type chemokine with a chemokine domain fused to a mucin-like stalk, a structure very similar to that of FNK [6, 7]. SR-PSOX/CXCL16 is selectively expressed on antigen-presenting cells (APCs) such as dendritic cells (DCs) and macrophages, and its receptor CXCR6 is expressed on naive $CD8^+$ T cells, natural killer T (NKT) cells, and type 1-polarized, activated $CD4^+$ and $CD8^+$ T cells [12–16]. It has been proposed that CXCL16 promotes the movement of T cells toward DCs in the splenic red pulp [12]. Furthermore, CXCR6-expressing effector T cells were found to be abundant in type 1 inflammatory lesions such as rheumatoid joints and inflamed livers [16].

DCs, which capture and process antigens to form major histocompatibility complex peptide complexes, function as

[1] Correspondence: Graduate School of Biostudies and Institute for Virus Research, Kyoto University, Shogoin Kawahara-cho 53, Sakyo-ku, Kyoto 606-8507, Japan. E-mail: syonehar@virus.kyoto-u.ac.jp

Received October 9, 2003; accepted October 14, 2003; doi: 10.1189/jlb.1003465.

professional APCs to T cells. After up-taking antigen and migrating from the periphery to the T cell areas of secondary lymphoid organs, DC contact can initiate primary immune responses via activation of resting T cells. In addition, contacts between DCs and T cells are essential to maintain and restart immune responses of previously activated T cells [17, 18]. Adhesion molecules such as lymphocyte function-associated antigen-3 (LFA-3)/CD2, LFA-1/intercellular adhesion molecule-1 (ICAM-1) and DC-specific ICAM-3-grabbing nonintegrin/ICAM-3 are reported to mediate interactions between DCs and T cells and to provide activation signals via DC–T cell adhesion [19, 20]. Notably, the membrane-anchored chemokine, FNK, whose molecular structure is similar to that of SR-PSOX/CXCL16, can directly function as an adhesion molecule for cells expressing its receptor CX_3CR1 [8, 9]. Here, we demonstrate that in a manner very similar to that of FNK, SR-PSOX also functions as a direct adhesion cell molecule for cells expressing its receptor CXCR6. The chemokine domain of SR-PSOX primarily mediates the adhesion of CXCR6-expressing cells. The adhesion is not inhibited by pertussis toxin (PTX), the Gαi protein inhibitor, although it effectively suppresses chemotaxis of CXCR6-expressing cells induced by SR-PSOX/CXCL16. Furthermore, the adhesion of CXCR6-expressing cells can be enhanced by treatment of SR-PSOX/CXCL16-expressing cells with a metalloprotease inhibitor, which increases the surface expression of SR-PSOX/CXCL16. Thus, SR-PSOX/CXCL16 may play an important role in interactions between DCs and T cells or NKT cells as a chemoattractant as well as a cell adhesion molecule.

MATERIALS AND METHODS

Materials and cells

PTX, wortmannin, and PD098059 were purchased from Calbiochem-Novabiochem (La Jolla, CA). EGTA was purchased from Sigma Chemical Co. (St. Louis, MO). Mouse-activated T cells expressing CXCR6 were prepared as described previously [12] with minor modifications. In brief, T cells (2×10^5 cells/ml) isolated from splenocyte suspensions by magnetic cell sorter were activated by cultivation with RPMI-1640 medium containing 10% fetal bovine serum (FBS) and mouse interleukin (IL)-2 (4 ng/ml) for 5 days in plastic plates precoated with anti-CD3 (2C11) and anti-CD28 (37.51; PharMingen, San Diego, CA). The activated T cells were then left to rest in RPMI-1640 medium containing 10% FBS and IL-2 (2 ng/ml) for 4 days and were used as CXCR6-expressing cells. Transfection of COS-7 cells was performed as described previously [10]. L1.2 murine pre-B cells stably expressing CXCR6 (L-CXCR6) or CX_3CR1 (L-CX_3CR1) were generated as reported previously [8].

Monoclonal anti-human (h)- and mouse (m)SR-PSOX antibodies

Female Lewis rats were immunized with mSR-PSOX-Fc fusion protein, produced by COS-7 cells, transfected with a fusion construct consisting of the extracellular domain of mSR-PSOX (amino acids 1–198) fused at its C terminus with an Fc fragment of human immunoglobulin G (IgG)1. Three days after the last immunization, spleen cells were fused with NS-1 mouse myeloma cells as described previously [21]. Finally, we generated an anti-mSR-PSOX monoclonal antibody (mAb) 12-81. Anti-hSR-PSOX mAb 22-19-12, 49-36, and 28-12 were generated as described previously [11].

Preparation of polyclonal anti-hSR-PSOX antibody

Synthetic peptides corresponding to amino acid residues 42–61 of hSR-PSOX were conjugated to Imject Maleimide-Activated mcKLH (Pierce, Rockford, IL). After the immunization of a rabbit with the conjugates, polyclonal antiserum was collected and purified using a column packed with peptide corresponding to amino acid residues 42–61 of hSR-PSOX.

SR-PSOX-FNK hybrid protein

Plasmids encoding SR-PSOX-FNK hybrid molecules were generated by polymerase chain reaction (PCR) and subsequent ligation of DNA fragments into pME18S [22] as described previously [21]. In brief, the following fragments were amplified by PCR using primers as indicated: DNA encoding the chemokine domain of hSR-PSOX (amino acids 1–118) using primers 5′-TCACTCGAGATGGCACCGGACTTGCGGCC-3′ and 5′-TCAGAATTCAGGAAGTAAATGCTTCTGGTGGC-3′; DNA encoding the chemokine domain of hFNK (amino acids 1–206) using 5′-TCACTCGAGAGCTCTGCCGCCTGGCTCTA-3′ and 5′-TCAGAATTCTAGGGCAGCAAGCCTGGCGGT-3′; DNA encoding the region containing the mucin, transmembrane, and cytoplasmic domains of hSR-PSOX (amino acids 120–254) using 5′-TCAGAATTCACCAGCCCCCAATTTCTCA-3′ and 5′-TCACTGCAGTCAGGTATTAGAGTCAGGTG-3′; and DNA encoding the region containing the mucin, transmembrane, and cytoplasmic domains of hFNK (amino acids 97–397) using 5′-TCAGAATTCACTCGAAATGGCGGCACCTT-3′ and 5′-TCACTGCAGACTAGACACAGGCCAGAGGA-3′. PCR fragments of the chemokine domain were digested with *Xho*I and *Eco*RI, and PCR fragments of the other domains were digested with *Eco*RI and *Pst*I. These digested fragments were ligated together into pME18S digested with *Xho*I and *Pst*I, and expression vectors for four kinds of SR-PSOX-FNK hybrids (S-S, S-F, F-S, and F-F, see Fig. 4A) were prepared. DNA encoding hSR-PSOX without the mucin domain (amino acids 119–205; Δmucin) was generated by ligating DNA fragments encoding the chemokine domain of hSR-PSOX and the transmembrane and cytoplasmic domains of hSR-PSOX, which were prepared at once by PCR using 5′-GCACAGGACCGGCACAGGAAGTAAATGCTT-3′, 5′-TCACTCGAGATGGCACGGCACTTGCGGCC-3′, and 5′-GCAGTGGCTGGTTAGTCCTA-3′ as primers. These PCR fragments digested with *Xho*I and *Hin*dIII and with adaptor fragments generated by digestion of pME18S with *Xho*I and *Hin*dIII were ligated together into *Hin*dIII-digested pME18S-SR-PSOX.

Chemotaxis and calcium mobilization assays

Chemotaxis assays using transwell plates with 5 μm pore size membrane (Corning Costar, Corning, NY) and calcium mobilization assays were performed as described previously [8]. In some experiments, cells were preincubated with PTX (500 ng/ml), wortmannin (100 nM), or PD098059 (50 μM) for 30 min at 37°C.

Cell adhesion assays

Cell adhesion to immobilized SR-PSOX or FNK was measured essentially as described previously [8]. In adhesion assays with immobilized chemokines, enzyme-linked immunosorbent assay (ELISA) plates (Corning Costar) were precoated with 10 nM chemokines fused with a secreted form of placental alkaline phosphatase (SEAP). L-CXCR6 cells or mouse-activated T cells were transferred to each well (5×10^4 cells/well) and incubated for 30 min at room temperature (RT). After being washed, adherent cells were quantified using Picogreen double-strand DNA quantitation reagent (Molecular Probes, Eugene, OR). In adhesion assays with chemokine-expressing cells, L-CXCR6 or mouse-activated T cells labeled with calcein acetoxymethyl ester (calcein-AM; Molecular Probes) were transferred to 12-well plates (5×10^5 cells/well), where COS-7 cells expressing SR-PSOX (COS-SR-PSOX cells) were preseeded. After incubation for 60 min at 37°C, nonadherent cells were removed by washing, and fluorescence intensity was measured using Wallac 1420 ARVO fluoroscan (Wallac, Turku, Finland). To analyze effects of various inhibitors, COS-SR-PSOX cells and L-CXCR6 cells were preincubated with PTX (500 ng/ml), wortmannin (100 nM), PD098059 (50 μM), or soluble (s)SR-PSOX-SEAP (20 nM) for 30 min at 37°C.

Expression analysis of SR-PSOX and CXCR6

For flow cytometric analysis of cell surface-expressed hSR-PSOX, cells were detached from dishes with 5 mM EDTA and incubated for 1 h on ice with 20 μg/ml anti-hSR-PSOX mAb, clone 22-19-12, 49-36, or 28-12 or control mouse IgG. After being washed, cells were incubated with 20 μg/ml fluorescein isothiocyanate (FITC)-conjugated anti-mouse IgG antibody (Cappel, Aurora, OH) on ice for 1 h. After two-times washes, cells were analyzed on an EPICS

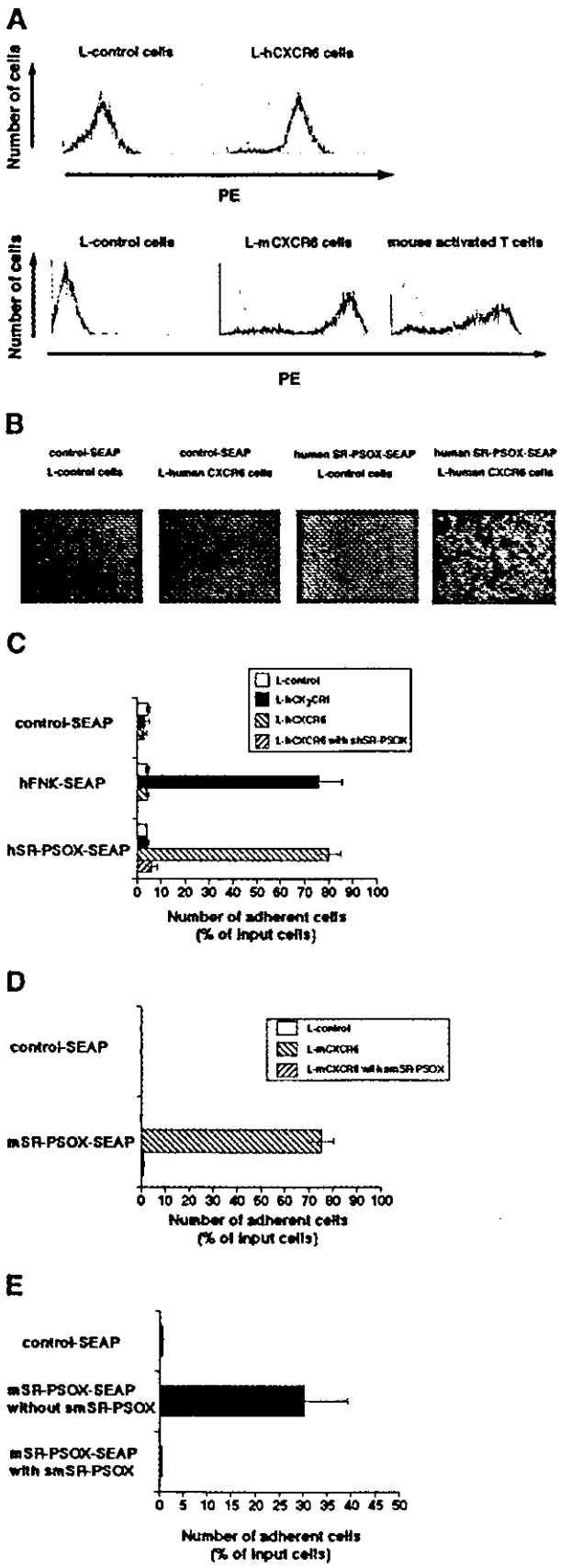

Fig. 1. Immobilized SR-PSOX/CXCL16 on plastic dish mediates cell adhesion of CXCR6-expressing cells. (A) Flow cytometric analysis. Surface expression of hCXCR6 on control murine L1.2 cells (L-control cells) and murine L-hCXCR6 cells was analyzed by flow cytometry after staining with anti-hCXCR6 mAb 56811 (bold line) or control IgG (dotted line). Surface expression of mCXCR6 on L-control cells, murine L-mCXCR6 cells, and mouse-activated T cells was analyzed by flow cytometry using SR-PSOX-Fc as described in Materials and Methods. Mouse-activated T cells were prepared by in vitro activation with CD3 and CD28 as described in Materials and Methods. (B–E) Assay of adhesion to immobilized SR-PSOX-SEAP on plastic culture dishes. L-control, L-hCXCR6, and L-hCX$_3$CR1 cells were transferred to plastic culture dishes precoated with control-SEAP, hSR-PSOX-SEAP, or hFNK-SEAP and were incubated for 30 min at RT (B and C). L-control and L-mCXCR6 cells (D) and mouse-activated T cells (E) were incubated in wells precoated with control SEAP or mSR-PSOX-SEAP and were incubated for 30 min at RT. After the washes of plates, adherent cells were observed under light microscopy (B) and quantified using Picogreen double-strand DNA quantitation reagent (C–E). In blocking experiments, shSR-PSOX and smSR-PSOX, respectively (20 nM), were preincubated with SR-PSOX-SEAP-coated plates, L-hCXCR6 or L-mCXCR6 cells, and mouse-activated T cells for 30 min. The data shown represent the mean ± SD from at least three independent experiments.

Elite (Coulter, Hialeah, FL). Flow cytometric analysis of cell surface-expressed mSR-PSOX was similarly performed using the anti-mSR-PSOX mAb 12-81. For flow cytometric analysis of cell surface-expressed hCXCR6, Fc receptors on cells were blocked by treatment with human IgG, and then cells were stained with phycoerythrin (PE)-labeled anti-hCXCR6 mAb (clone 56811). For flow cytometric analysis of mCXCR6, Fc receptors were blocked by FITC-labeled anti-CD16/CD32 (PharMingen), and then cells were stained with SR-PSOX-Fc and PE-labeled goat anti-human Fcγ as described previously [12].

Quantification of SR-PSOX by ELISA

ELISA plates were coated with the monoclonal anti-SR-PSOX antibody 28-12 (10 μg/ml, 50 μl/well) by incubating for 2 h at 37°C. After three-times washes with phosphate-buffered saline (PBS) containing 0.1% Tween 20, the plates were blocked with fourfold-diluted BlockAce (Dainippon Seiyaku, Osaka, Japan) for 1 h at RT. After three more washes, appropriately diluted samples or standards (50 μl/well) were loaded and incubated for 2 h at RT. After another three-times washes, rabbit polyclonal anti-SR-PSOX antibody (50 μl/well) against synthetic peptides corresponding to amino acid residues 42–61 of hSR-PSOX (10 μg/ml) was transferred to the plate and incubated for 1 h at RT. After three-times washes with PBS containing 0.1% Tween 20, anti-rabbit IgG–horseradish peroxidase (50 μl/well), which does not cross-react with mouse IgG (Amersham Biosciences, Little Chalfont, UK), was transferred and incubated for 30 min at RT. After another three washes with PBS containing 0.1% Tween 20, tetramethylbenzidine substrate buffer (100 μl/well; Dako, Carpinteria, CA) was transferred to each well. After incubation for 5–30 min at RT, stop solution (100 μl/well) was transferred to each well, and the optical density (O.D.) at 450 nm was determined using Wallac 1420 ARVO fluoroscan (Wallac).

Preparation of SR-PSOX-containing samples for ELISA

COS-SR-PSOX cells in 24-well tissue-culture plates were cultured for 24 h with serum-free medium in the presence or absence of the metalloproteinase inhibitor GM6001 (10 μM). Then, culture supernatants were collected for quantification of sSR-PSOX. After being washed with PBS, cells were lysed for 30 min with lysis buffer (PBS containing 1% Nonidet P-40, 0.5% sodium deoxycholate, 0.1% sodium dodecyl sulfate, 0.1 mM phenylmethylsulfonyl fluoride, and 1% protease inhibitor mixture). After clarification of the culture supernatants and cell lysates by centrifugation, ELISA quantified the SR-PSOX. The data shown represent the mean ± SD from at least three independent experiments.

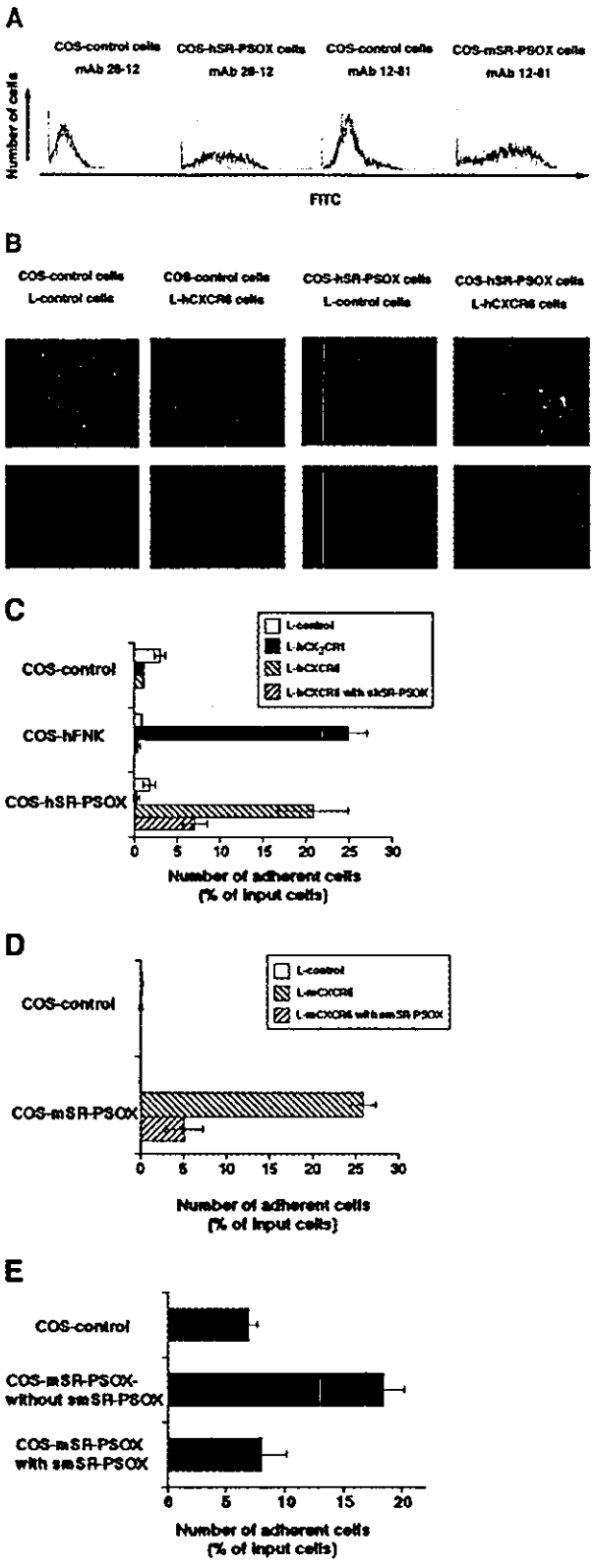

Fig. 2. SR-PSOX/CXCL16-expressing cells mediate adhesion of CXCR6-expressing cells. (A) Flow cytometric analysis. COS-7 cells were transfected with control vector (COS-control cells) or hSR-PSOX (COS-hSR-PSOX cells) or mSR-PSOX (COS-mSR-PSOX) cells, respectively. The transient expression of hSR-PSOX or mSR-PSOX on these COS-7 cells was analyzed by flow cytometry after staining with anti-hSR-PSOX mAb 28-12 or anti-mSR-PSOX mAb 12-81 (bold lines) or with control antibody (dotted line) as described in Materials and Methods. (B–E) Adhesion assay with SR-PSOX-expressing COS-7 cells. L-control, L-hCXCR6, and L-hCX$_3$CR1, labeled with calcein-AM, were incubated with COS-control, COS-hSR-PSOX, or COS-hFNK cells for 60 min at 37°C (B and C). L-mCXCR6 (D) or mouse-activated T cells (E) were labeled with calcein-AM and then incubated with COS-control or COS-mSR-PSOX cells for 60 min at 37°C. After the washes of plates, adherent cells were observed under light microscopy (upper panels) and fluorescence microscopy (lower panels; B), and fluorescence intensity was quantified as described in Materials and Methods (C–E). In blocking experiments, shSR-PSOX or smSR-PSOX (20 nM) was preincubated with COS-SR-PSOX cells and L-CXCR6 or mouse-activated T cells for 30 min. The data shown represent the mean ± SD from at least three independent experiments.

RESULTS

Immobilized SR-PSOX/CXCL16 on plastic culture dish mediates adhesion of CXCR6-expressing cells

SR-PSOX/CXCL16 is a transmembrane protein with an N-terminal CXC chemokine domain fused to a mucin-like stalk [10–13]. This structure is very similar to that of another transmembrane-type chemokine, FNK [6, 7]. The membrane-anchored form of FNK has been demonstrated to induce firm adhesion of cells expressing its receptor CX$_3$CR1 in static and flow conditions [8, 9]. We, therefore, examined whether the membrane-anchored SR-PSOX/CXCL16 was also capable of mediating firm adhesion of CXCR6-expressing cells. First, we examined whether SR-PSOX-SEAP immobilized to plastic culture dishes was capable of trapping L-hCXCR6 cells, whose expression of CXCR6 was confirmed by flow cytometry (**Fig. 1A**). As shown in Figure 1, B and C, L-hCXCR6 cells indeed bound to immobilized hSR-PSOX-SEAP. Conversely, L-hCX$_3$CR1 cells did not bind to hSR-PSOX-SEAP but bound to hFNK-SEAP. Neither L-hCXCR6 cells nor L-hCX$_3$CR1 cells bound to control-immobilized SEAP. The adhesion of L-hCXCR6 cells was inhibited by shSR-PSOX. Similarly, L-mCXCR6 cells, whose expression of mCXCR6 was confirmed by flow cytometry (Fig. 1A) and reverse transcriptase-PCR (data not shown), selectively bound to immobilized mSR-PSOX-SEAP in a manner sensitive to smSR-PSOX (Fig. 1D). We further demonstrated specific adhesion of normal mouse T cells expressing CXCR6 (Fig. 1A), which were prepared by activation in vitro with anti-CD3 and anti-CD28, to immobilized mSR-PSOX-SEAP, again in a manner sensitive to smSR-PSOX (Fig. 1E).

Adhesion of CXCR6-expressing cells to SR-PSOX/CXCL16-expressing cells

We then examined adhesion of CXCR6-expressing cells to the membrane-anchored chemokines expressed on COS-7 cells. L-hCXCR6 cells selectively bound to COS-7 cells transfected with hSR-PSOX/CXCL16 (COS-hSR-PSOX cells), whose expression was confirmed by flow cytometry (**Fig. 2A**), and L-hCX$_3$CR1 cells selectively bound to those expressing FNK (COS-hFNK cells; Fig. 2, B and C). Adhesion of L-hCXCR6 cells to COS-hSR-PSOX cells was inhibited by shSR-PSOX. Neither L-CXCR6 nor L-CX$_3$CR1 bound to control COS-7 cells (COS-control cells). As shown in Figure 2, D and E, L-mCXCR6 cells and mouse-activated T cells selectively

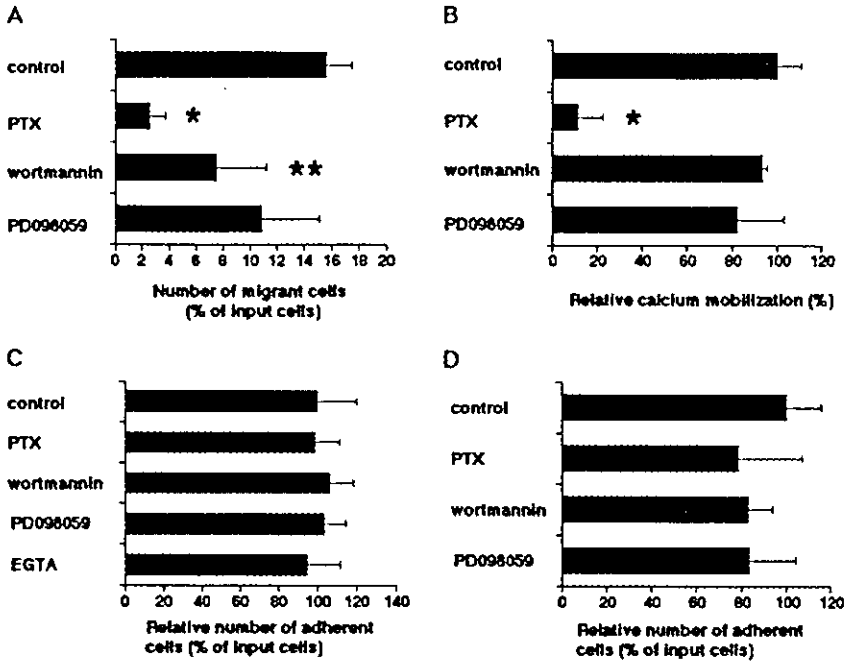

Fig. 3. Signal transduction through chemokine receptor is not required for SR-PSOX-CXCR6-induced cell adhesion. (A) Examination of chemotaxis by standard transwell assays. hSR-PSOX-SEAP (10 nM) was analyzed for its chemotactic activity against L-hCXCR6 cells preincubated with PTX (500 ng/ml), wortmannin (100 nM), or PD098059 (50 μM) for 30 min. (B) Calcium mobilization assay. L-hCXCR6 cells preincubated with or without the indicated inhibitors for 30 min, were loaded with fura-PE3-AM and stimulated with hSR-PSOX-SEAP (10 nM). The intracellular concentration of calcium was monitored using fluorescence ratio (F340/F380). Values in the absence of inhibitor were set as 100%. (C, D) Cell adhesion assays. Adhesion of L-hCXCR6 cells to hSR-PSOX-SEAP-coated plates (C) or COS-hSR-PSOX cells (D) was measured as described in Figures 1 and 2. Cells were preincubated with or without the indicated inhibitors for 30 min. Values in the absence of inhibitor were set as 100%. (A–D) The data shown represent the mean ± SD from at least three independent experiments. *, $P < 0.01$; **, $P < 0.05$.

bound to COS-mSR-PSOX/CXCL16, whose expression was confirmed by flow cytometry (Fig. 2A). Collectively, similar to the membrane-anchored FNK [8, 9], the membrane-anchored SR-PSOX/CXCL16 was indeed capable of mediating adhesion of cells expressing its receptor CXCR6.

CXCR6-mediated signal transduction is not required for adhesion induced by SR-PSOX/CXCL16

As shown in **Figure 3, A** and **B**, PTX, a potent inhibitor of the Gαi class of G proteins, effectively suppressed responses of L-hCXCR6 cells to hSR-PSOX-SEAP in chemotaxis and calcium-mobilization assays as described previously [12]. Chemotaxis but not calcium mobilization was also slightly inhibited by the phosphatidylinositol-3 kinase (PI-3K) inhibitor wortmannin, and the mitogen-activated protein kinase kinase inhibitor PD098059 did not show any significant inhibition of chemotaxis or calcium mobilization. The effects of wortmannin on chemotaxis and calcium mobilization are very similar to those shown in T lymphoblasts stimulated with another chemokine, stromal cell-derived factor 1/CXCL12 [23]. Conversely, the adhesion of L-hCXCR6 cells to immobilized hSR-PSOX-SEAP or COS-hSR-PSOX cells was not inhibited by PTX, wortmannin, or PD098059 (Fig. 3, C and D). We also confirmed that EGTA did not suppress the adhesion of L-hCXCR6 cells to hSR-PSOX-SEAP-coated plates (Fig. 3C). Therefore, the adhesion of CXCR6-expressing cells to SR-PSOX/CXCL16 did not require signaling via PTX-sensitive G proteins or PI-3K downstream of chemokine receptors or calcium-dependent activation of integrins. These data were very similar to those reported for adhesion of CX_3CR1-expressing cells mediated by membrane-anchored FNK [8]. In addition,

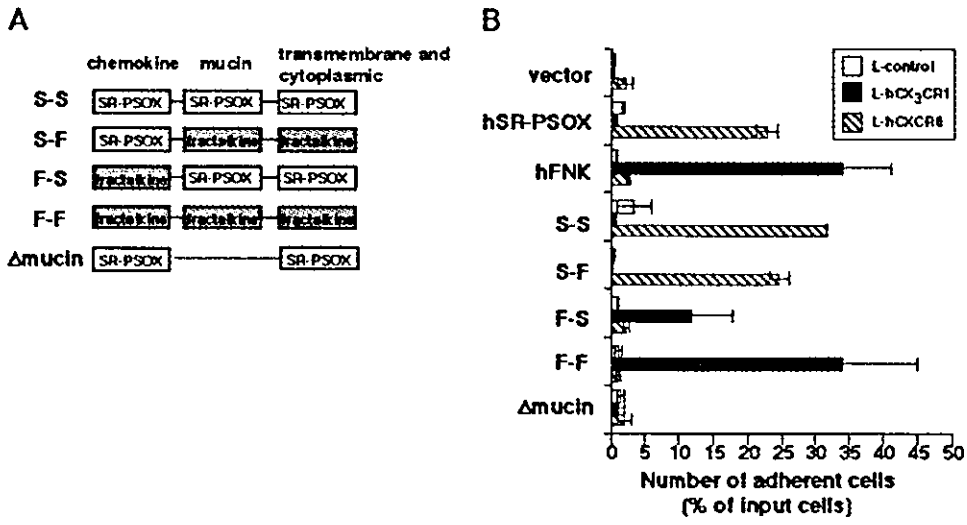

Fig. 4. Domain analyses of hSR-PSOX. (A) Schematic illustration of hSR-PSOX-FNK hybrids. The preparation of cDNA encoding these hybrid molecules was described in Materials and Methods. ΔMucin indicates hSR-PSOX without the mucin domain. (B) Adhesion assay. Adhesion of L-control, L-hCXCR6, and L-hCX_3CR1 cells to COS-7 cells transfected with the indicated hSR-PSOX-FNK hybrid was evaluated as in Figure 2. The data shown represent the mean ± SD from at least three independent experiments.

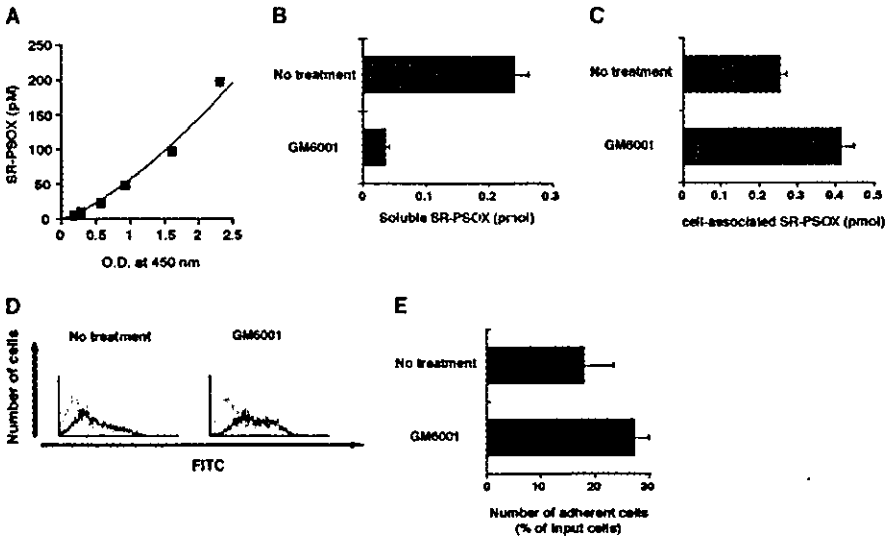

Fig. 5. Effects of metalloproteinase inhibitor GM6001 on expression and adhesion-inducing activity of SR-PSOX/CXCL16. (A) Standard curve for quantification of hSR-PSOX by ELISA. The standard curve was drawn by using hSR-PSOX-SEAP as described in Materials and Methods. The data shown represent the average of the duplicate. (B) Effect of metalloproteinase inhibitor on the release of shSR-PSOX. shSR-PSOX generated in the culture medium of COS-hSR-PSOX cells was quantified by ELISA after cultivation for 24 h with or without the metalloproteinase inhibitor GM6001 (10 μM). COS-control cells showed an undetectable level of shSR-PSOX (data not shown). The data represent the mean ± SD from at least three independent experiments. $P < 0.01$. (C) Effect of metalloproteinase inhibitor on the amount of cell-associated hSR-PSOX. ELISA determined the amounts of cell-associated hSR-PSOX in solubilized COS-hSR-PSOX cells after cultivation for 24 h with or without GM6001 (10 μM). COS-control cells showed an undetectable level of cell-associated hSR-PSOX (data not shown). The data shown represent the mean ± SD from at least three independent experiments. $P < 0.01$. (D) Effect of metalloproteinase inhibitor on the cell-surface expression of hSR-PSOX. Representative flow cytometric data of hSR-PSOX on COS-hSR-PSOX cells were shown after cultivation for 24 h with or without GM6001 (10 μM). The surface expression of hSR-PSOX on COS-hSR-PSOX cells was analyzed by flow cytometry after staining with anti-SR-PSOX mAb 22-19-12 (bold line) or control IgG (dotted line). (E) Adhesion assay for COS-7 cells. The adhesion of L-hCXCR6 cells to COS-hSR-PSOX cells after cultivation for 24 h with or without GM6001 (10 μM) was measured as in Figure 2. $P < 0.05$.

L-hCXCR6 cells were shown to bind not only to the immobilized extracellular domain of SR-PSOX on plastic culture dishes (Fig. 1) but also to the cytoplasmic domain-truncated SR-PSOX expressed on COS-7 cells (data not shown). These results indicate that the cytoplasmic domain of SR-PSOX is not required for adhesion between cells expressing SR-PSOX and those expressing CXCR6, although SR-PSOX has a predictable phosphorylation site in the cytoplasmic domain [12].

Domain analyses of SR-PSOX for adhesion of CXCR6-expressing cells

SR-PSOX/CXCL16 and FNK have two extracellular domains, namely a chemokine domain and a mucin-stalk domain. The chemokine domain of SR-PSOX without the mucin-stalk domain efficiently induced chemotaxis of CXCR6-expressing cells (data not shown). To clarify which domains of SR-PSOX were necessary for the adhesion of CXCR6-expressing cells, we generated SR-PSOX-FNK hybrids by shuffling the chemokine domains and mucin domains of hSR-PSOX and FNK, as described in Materials and Methods (**Fig. 4A**). COS-7 cells were transfected with the expression vectors for these hybrid proteins, and their similar levels of surface expression were confirmed by flow cytometry [11]. L-hCXCR6 cells but not L-hCX_3CR1 cells bound to COS-7 cells expressing the hybrid with the chemokine domain of hSR-PSOX and the mucin domain of FNK (Fig. 4B), and L-hCX_3CR1 cells but not L-hCXCR6 cells bound to COS-7 cells expressing the hybrid with the chemokine domain of FNK and the mucin domain of hSR-PSOX/CXCL16. It is interesting that COS-7 cells expressing SR-PSOX without its mucin domain had impaired adhesion activity (Fig. 4B), although its cell-surface expression was confirmed by flow cytometry [11]. These results are very similar to those reported for cell adhesion mediated by membrane-anchored FNK [8, 24, 25] and indicate that the specificity for CXCR6 is determined by the chemokine domain of SR-PSOX/CXCL16, and the mucin domain of SR-PSOX/CXCL16 is necessary for the effective presentation of the chemokine domain.

Enhancing effect of metalloproteinase inhibitor on cell adhesion mediated by SR-PSOX/CXCL16

FNK was reported to be prototypically released from the cell surface by the function of metalloproteinase, and the soluble form thus generated functions as a chemoattractant similar to other members of the chemokine family [26, 27]. Given the possibility of a similar processing of the membrane-anchored SR-PSOX/CXCL16, we examined the effect of metalloproteinase inhibitor on the ratio of soluble-to-membrane-bound forms of SR-PSOX/CXCL16. The release of sSR-PSOX from COS-hSR-PSOX cells was clearly inhibited by a metalloproteinase inhibitor GM6001, and cell-surface and cell-associated hSR-PSOX expression was increased by the treatment (**Fig. 5, A–D**). This prompted us to examine the effect of the metalloproteinase inhibitor on SR-PSOX/CXCL16-mediated adhesion activity. As expected from the increased cell-surface expression of SR-PSOX, more L-hCXCR6 cells were found to bind to GM6001-treated COS-hSR-PSOX cells than untreated COS-hSR-PSOX cells (Fig. 5E).

DISCUSSION

As FNK, the first reported transmembrane chemokine, mediates not only chemotaxis but also adhesion in CX_3CR1-expressing cells, SR-PSOX/CXCL16, the second reported transmembrane chemokine, can also be predicted to function as a

cell adhesion molecule for CXCR6-expressing cells. Recently, we reported in brief that immobilized SR-PSOX/CXCL16 induces direct adhesion of CXCR6-expressing plasma cells [28], although we did not examine the mechanism in detail. In the present study, we precisely showed the direct adhesion of CXCR6-expressing cells not only to immobilized SR-PSOX/CXCL16 on plastic culture dish (Fig. 1) but also to SR-PSOX/CXCL16-expressing cells (Fig. 2). In addition, the chemokine domain of SR-PSOX was proven to determine the specificity for CXCR6-expressing cells (Fig. 4). Furthermore, we demonstrated that metalloproteinase regulates the release of sSR-PSOX/CXCL16 from the membrane-anchored form and thus down-regulates the activity of SR-PSOX-expressing cells to bind CXCR6-expressing cells (Fig. 5).

SR-PSOX and CXCR6 regulate the processes of chemotaxis as well as direct adhesion. The Gαi protein blocker, PTX, can inhibit CXCR6-mediated migratory activity, however, by indicating that activation of Gαi protein is necessary for the induction of the chemotactic response. In contrast, adhesion occurs even in the presence of PTX (Fig. 3). These findings are similar to those reported for FNK [8]. Indeed, the adhesion between cells expressing SR-PSOX and those expressing CXCR6 can be induced, independent of the activation of G protein or the activation of integrins.

COS-7 cells expressing SR-PSOX without its mucin domain were shown to have impaired adhesion activity, although COS-7 cells expressing a hybrid with the chemokine domain of hSR-PSOX and the mucin domain of FNK efficiently bind L-hCXCR6 cells (Fig. 4). These results indicate that the chemokine domain of SR-PSOX/CXCL16 only determines specificity for CXCR6, and the mucin domain of SR-PSOX/CXCL16 is necessary for the efficient adhesion. The mucin domain of FNK was also shown to contribute to the efficient adhesion activity of CX_3CR1-expressing cells (Fig. 4B). However, the mucin domain is unlikely to determine the specificity of the cell adhesion directly, as the mucin domain of FNK when substituted for that of SR-PSOX is functional in terms of adhesion activity for CXCR6-expressing cells. Cell adhesion is mediated by direct protein–protein interactions, which may require some distance from the cell surface as discussed previously [8, 24, 25]. Thus, the mucin domain of SR-PSOX/CXCL16 may function as a necessary presenting structure of the chemokine domain, which provides some distance from the cell surface for the chemokine domain to interact with CXCR6 on the surface of target cells.

We have shown the multiple functions of SR-PSOX/CXCL16, which include the scavenger receptor activity, the chemotaxis-inducing activity, and the direct cell-adhesion activity. We therefore suggest that SR-PSOX/CXCL16 plays multifunctional roles in DCs. The soluble form of SR-PSOX/CXCL16 generated by metalloproteinase cleavage recruits CXCR6-expressing, activated T cells and NKT cells via its chemotactic activity in cooperation with other chemokines. Then, the membrane-anchored form of SR-PSOX/CXCL16 on DCs can function as a cell-surface adhesion molecule for CXCR6-expressing T and NKT cells in cooperation with other adhesion molecules. Such adhesion may lead to bidirectional stimulatory signals and may contribute to the formation of docking sites for the activation of antigen-specific, primary and secondary T cell responses. Thus, SR-PSOX/CXCL16 may play a role in DC functions for primary and secondary immune responses. These possibilities are currently under investigation.

ACKNOWLEDGMENTS

This work was supported in part by Grants-in-Aid from the Ministry of Education, Culture, Sports, Science and Technology of the Japanese Government. We thank Drs. K. Sakamaki and K. K. Lee for helpful comments.

REFERENCES

1. Zlotnik, A., Yoshie, O. (2000) Chemokines: a new classification system and their role in immunity. *Immunity* **12**, 121–127.
2. Goda, S., Imai, T., Yoshie, O., Yoneda, O., Inoue, H., Nagano, Y., Okazaki, T., Imai, H., Bloom, E. T., Domae, N., Umehara, H.. (2000) CX3C-chemokine, fractalkine-enhanced adhesion of THP-1 cells to endothelial cells through integrin-dependent and -independent mechanisms. *J. Immunol.* **164**, 4313–4320.
3. Campbell, J. J., Hedrick, J., Zlotnik, A., Siani, M. A., Thompson, D. A., Butcher, E. C. (1998) Chemokines and the arrest of lymphocytes rolling under flow conditions. *Science* **279**, 381–384.
4. Pachynski, R. K., Wu, S. W., Gunn, M. D., Erle, D. J. (1998) Secondary lymphoid-tissue chemokine (SLC) stimulates integrin α 4 β 7-mediated adhesion of lymphocytes to mucosal addressin cell adhesion molecule-1 (MAdCAM-1) under flow. *J. Immunol.* **161**, 952–956.
5. Campbell, J. J., Qin, S., Bacon, K. B., Mackay, C. R., Butcher, E. C. (1996) Biology of chemokine and classical chemoattractant receptors: differential requirements for adhesion-triggering versus chemotactic responses in lymphoid cells. *J. Cell Biol.* **134**, 255–266.
6. Pan, Y., Lloyd, C., Zhou, H., Dolich, S., Deeds, J., Gonzalo, J. A., Vath, J., Gosselin, M., Ma, J., Dussault, B., Woolf, E., Alperin, G., Culpepper, J., Gutierrez-Ramos, J. C., Gearing, D. (1997) Neurotactin, a membrane-anchored chemokine upregulated in brain inflammation. *Nature* **387**, 611–617.
7. Bazan, J. F., Bacon, K. B., Hardiman, G., Wang, W., Soo, K., Rossi, D., Greaves, D. R., Zlotnik, A., Schall, T. J. (1997) A new class of membrane-bound chemokine with a CX3C motif. *Nature* **385**, 640–644.
8. Imai, T., Hieshima, K., Haskell, C., Baba, M., Nagira, M., Nishimura, M., Kakizaki, M., Takagi, S., Nomiyama, H., Schall, T. J., Yoshi, O. (1997) Identification and molecular characterization of fractalkine receptor CX3CR1, which mediates both leukocyte migration and adhesion. *Cell* **91**, 521–530.
9. Fong, A. M., Robinson, L. A., Steeber, D. A., Tedder, T. F., Yoshie, O., Imai, T., Patel, D. D. (1998) Fractalkine and CX3CR1 mediate a novel mechanism of leukocyte capture, firm adhesion, and activation under physiologic flow. *J. Exp. Med.* **188**, 1413–1419.
10. Shimaoka, T., Kume, N., Minami, M., Hayashida, K., Kataoka, H., Kita, T., Yonehara, S. (2000) Molecular cloning of a novel scavenger receptor for oxidized low density lipoprotein, SR-PSOX, on macrophages. *J. Biol. Chem.* **275**, 40663–40666.
11. Shimaoka, T., Nakayama, T., Kume, N., Takahashi, S., Yamaguchi, J., Minami, M., Hayashida, K., Kita, T., Ohsumi, J., Yoshie, O., Yonehara, S. (2003) Cutting edge: SR-PSOX/CXC chemokine ligand 16 mediates bacterial phagocytosis by APCs through its chemokine domain. *J. Immunol.* **171**, 1647–1651.
12. Matloubian, M., David, A., Engel, S., Ryan, J. E., Cyster, J. G. (2000) A transmembrane CXC chemokine is a ligand for HIV-coreceptor Bonzo. *Nat. Immunol.* **1**, 298–304.
13. Wilbanks, A., Zondlo, S.'C., Murphy, K., Mak, S., Soler, D., Langdon, P., Andrew, D. P., Wu, L., Briskin, M. (2001) Expression cloning of the STRL33/BONZO/TYMSTRligand reveals elements of CC, CXC, and CX3C chemokines. *J. Immunol.* **166**, 5145–5154.
14. Deng, H. K., Unutmaz, D., KewalRamani, V. N., Littman, D. R. (1997) Expression cloning of new receptors used by simian and human immunodeficiency viruses. *Nature* **388**, 296–300.
15. Liao, F., Alkhatib, G., Peden, K. W., Sharma, G., Berger, E. A., Farber, J. M. (1997) STRL33, a novel chemokine receptor-like protein, functions

as a fusion cofactor for both macrophage-tropic and T cell line-tropic HIV-1. *J. Exp. Med.* **185,** 2015–2023.
16. Kim, C. H., Kunkel, E. J., Boisvert, J., Johnston, B., Campbell, J. J., Genovese, M. C., Greenberg, H. B., Butcher, E. C. (2001) Bonzo/CXCR6 expression defines type 1-polarized T-cell subsets with extralymphoid tissue homing potential. *J. Clin. Invest.* **107,** 595–601.
17. Banchereau, J., Steinman, R. M. (1998) Dendritic cells and the control of immunity. *Nature* **392,** 245–252.
18. Guermonprez, P., Valladeau, J., Zitvogel, L., Thery, C., Amigorena, S. (2002) Antigen presentation and T cell stimulation by dendritic cells. *Annu. Rev. Immunol.* **20,** 621–667.
19. Bleijs, D. A., Geijtenbeek, T. B., Figdor, C. G., van Kooyk, Y. (2001) DC-SIGN and LFA-1: a battle for ligand. *Trends Immunol.* **22,** 457–463.
20. Montoya, M. C., Sancho, D., Vicente-Manzanares, M., Sanchez-Madrid, F. (2002) Cell adhesion and polarity during immune interactions. *Immunol. Rev.* **186,** 68–82.
21. Yonehara, S., Ishii, A., Yonehara, M. (1989) A cell-killing monoclonal antibody (anti-Fas) to a cell surface antigen co-downregulated with the receptor of tumor necrosis factor. *J. Exp. Med.* **169,** 1747–1756.
22. Sakamaki, K., Miyajima, I., Kitamura, T., Miyajima, A. (1992) Critical cytoplasmic domains of the common β subunit of the human GM-CSF, IL-3 and IL-5 receptors for growth signal transduction and tyrosine phosphorylation. *EMBO J.* **11,** 3541–3549.
23. Sotsios, Y., Whittaker, G. C., Westwick, J., Ward, S. G. (1999) The CXC chemokine stromal cell-derived factor activates a Gi-coupled phosphoinositide 3-kinase in T lymphocytes. *J. Immunol.* **163,** 5954–5963.
24. Fong, A. M., Erickson, H. P., Zachariah, J. P., Poon, S., Schamberg, N. J., Imai, T., Patel, D. D. (2000) Ultrastructure and function of the fractalkine mucin domain in CX(3)C chemokine domain presentation. *J. Biol. Chem.* **275,** 3781–3786.
25. Haskell, C. A., Cleary, M. D., Charo, I. F. (2000) Unique role of the chemokine domain of fractalkine in cell capture. Kinetics of receptor dissociation correlate with cell adhesion. *J. Biol. Chem.* **275,** 34183–34189.
26. Tsou, C. L., Haskell, C. A., Charo, I. F. (2001) Tumor necrosis factor-α-converting enzyme mediates the inducible cleavage of fractalkine. *J. Biol. Chem.* **276,** 44622–44626.
27. Garton, K. J., Gough, P. J., Blobel, C. P., Murphy, G., Greaves, D. R., Dempsey, P. J., Raines, E. W. (2001) Tumor necrosis factor-α-converting enzyme (ADAM17) mediates the cleavage and shedding of fractalkine (CX3CL1). *J. Biol. Chem.* **276,** 37993–38001.
28. Nakayama, T., Hieshima, K., Izawa, D., Tatsumi, Y., Kanamaru, A., Yoshie, O. (2003) Cutting edge: profile of chemokine receptor expression on human plasma cells accounts for their efficient recruitment to target tissues. *J. Immunol.* **170,** 1136–1140.

Available online at www.sciencedirect.com
SCIENCE DIRECT®
Biochemical and Biophysical Research Communications 322 (2004) 700–704
BBRC
www.elsevier.com/locate/ybbrc

Direct demonstration of involvement of the adaptor protein ShcA in the regulation of Ca^{2+}-induced platelet aggregation☆

Tomohito Higashi[a], Akira Yoshioka[b,1], Ryutaro Shirakawa[a], Arata Tabuchi[b], Hiroaki Nishioka[b,2], Toru Kita[a], Hisanori Horiuchi[a,*]

[a] *Department of Cardiovascular Medicine, Graduate School of Medicine, Kyoto University, Kyoto 606-8507, Japan*
[b] *Geriatric Medicine, Graduate School of Medicine, Kyoto University, Kyoto 606-8507, Japan*

Received 20 May 2004

Abstract

Platelet aggregation is mediated by conformational change of integrin $\alpha_{IIb}\beta_3$. Tyrosine-phosphorylation of cytoplasmic domain of β_3 upon platelet activation has been demonstrated to play a critical role in this process. Recently, the adaptor protein ShcA has been shown to bind to the tyrosine-phosphorylated β_3, while it remains open whether ShcA plays any role in platelet aggregation. Here, we show that ShcA bound to tyrosine-phosphorylated β_3-tail peptide through its phosphotyrosine-binding domain in vitro. Then, we examined the involvement of ShcA in platelet aggregation by a previously established in vitro assay using platelets permeabilized with streptolysin-O, where exogenous addition of platelet cytosol is required for reconstitution of the Ca^{2+}-induced aggregation. When ShcA was specifically depleted with anti-ShcA antibody from the cytosol, this ShcA-depleted cytosol lost the aggregation-supporting activity, which was rescued by addition of purified recombinant ShcA. Thus, ShcA is essential for the Ca^{2+}-induced platelet aggregation.

Keywords: Platelet; Aggregation; Integrin; ShcA; Streptolysin-O; Phosphotyrosine-binding domain

Platelet aggregation is mediated by conformational change of integrin $\alpha_{IIb}\beta_3$ which is regulated by signals at its short cytoplasmic tails [1,2] that consist of 20 amino acids in α_{IIb} subunit and 47 in β_3 subunit [3]. Two tyrosine residues in β_3-tail are known to be phosphorylated during platelet activation [4] and platelets bearing mutations at these tyrosine residues exhibit impaired aggregation [5], indicating that these tyrosine residues are important for platelet aggregation. So far, myosin [6] and the adaptor protein ShcA [7] have been identified as tyrosine-phosphorylation-dependent β_3-tail binding proteins.

ShcA is the essential adaptor protein containing two phosphotyrosine-binding domains, the phosphotyrosine-binding (PTB) domain and Src-homology 2 (SH2) domain (Fig. 1A) [8]. ShcA mediates signals involved in cell growth [9] and cytoskeletal organization [10]. Accordingly, ShcA-deficient mice are embryonic lethal due to severe defects in heart development and establishment of mature blood vessels [10]. Upon platelet aggregation, ShcA has been demonstrated to be co-immunoprecipitated with tyrosine-phosphorylated $\alpha_{IIb}\beta_3$ [3] and to be phosphorylated at its tyrosine residues [11]. In platelets

☆ *Abbreviations:* PTB, phosphotyrosine-binding; SH2, Src-homology 2; PCR, polymerase chain reaction; GST, glutathione *S*-transferase; SLO, streptolysin-O; BSA, bovine serum albumin, SDS–PAGE, sodium dodecyl sulfate–polyacrylamide gel electrophoresis; CH1, collagen-homology 1.

* Corresponding author. Fax: +81 75 751 3574.
E-mail address: horiuchi@kuhp.kyoto-u.ac.jp (H. Horiuchi).
[1] Present address: Department of Internal Medicine, Mitsubishi Kyoto Hospital, 615-8087 Kyoto, Japan.
[2] Present address: Sir William Dunn School of Pathology, University of Oxford, South Parks Rd., Oxford OX1 3RE, UK.

0006-291X/$ - see front matter © 2004 Elsevier Inc. All rights reserved.
doi:10.1016/j.bbrc.2004.07.177